The unique synaptic circuitry of specialized olfactory glomeruli in *Drosophila melanogaster*

Lydia Gruber[1], Rafael Cantera[2], Markus William Pleijzier[3], Michael Steinert[4], Thomas Pertsch[4], Bill S. Hansson[1#], Jürgen Rybak [1#]

1 Max Planck Institute for Chemical Ecology, Department of Evolutionary Neuroethology, 07745 Jena, Germany
2 Instituto de Investigaciones Biológicas Clemente Estable, Departamento de Biología del Neurodesarrollo, 11600 Montevideo, Uruguay
3 Neurobiology Division, MRC Laboratory of Molecular Biology, Cambridge, CB2 0QH, England, United Kingdom
4 Institute of Applied Physics, Abbe Center of Photonics, Friedrich Schiller University Jena, Albert Einstein Strasse 15, 07745 Jena, Germany

# contributed equally
*Correspondence: Lydia Gruber (lgruber@ice.mpg.de) and Jürgen Rybak (jrybak@ice.mpg.de)

Keywords: olfactory circuitry, DA2, DL5, connectome*, Drosophila melanogaster*, FIB-SEM, synapses, sensory lateralization

ABSTRACT

In the *Drosophila* olfactory system most odorants are encoded in the antennal lobe in a combinatory way, activating several glomerular circuits. However, odorants of particular ecological role for the fly are encoded through activation of a single specialized olfactory pathway. Comparative analyses of densely reconstructed connectomes of one broadly tuned glomerulus (DL5) and one narrowly tuned glomerulus (DA2) gained detailed insight into the variations of synaptic circuitries of glomeruli with different computational tasks. Our approach combined laser-branding of glomeruli of interest with volume based focused ion beam-scanning electron microscopy (FIB-SEM) to enable precise targeting and analysis of the two glomeruli. We discovered differences in their neuronal innervation, synaptic composition and specific circuit diagrams of their major cell types: olfactory sensory neurons (OSNs), uniglomerular projection neurons (uPNs) and multiglomerular neurons (MGNs). By comparing our data with a previously mapped narrowly tuned glomerulus (VA1v), we identified putative generic features of narrowly tuned glomerular circuits, including higher density of neuronal fibers and synapses, lower degree of OSN lateralization, stronger axo-axonic connections between OSNs, dendro-dendritic connections between many uPNs, and lower degree of presynaptic inhibition on OSN axons. In addition, this work revealed that the dendrites of the single uPN in DL5 contain a substantial amount of autapses interconnecting distant regions of the dendritic tree**.** The comparative analysis of glomeruli allows to formulate synaptic motifs implemented in olfactory circuits with different computational demands.

INTRODUCTION

Olfaction is an anatomically shallow sensory system. In mammals and invertebrates just one synapse separates the sensory periphery from the central brain (Dolan *et al.*, 2018; Liang *et al.*, 2010; Owald *et al.*, 2015; Shepherd, 2011; Su *et al.*, 2009). In the olfactory system of *Drosophila melanogaster*, the first relay station of synaptic transmission is the antennal lobe (AL), which has a circuit architecture homologous to that of the vertebrate olfactory bulb (Boeckh *et al.*, 1990; Sachse *et al.*, 2021; Shepherd *et al.*, 2021). The fly AL consists of approximately 58 spherical compartments, called glomeruli, which can be distinguished by size, shape and location (Bates *et al.*, 2020; Gao *et al.*, 2000; Grabe *et al.*, 2015; Laissue *et al.*, 1999; Vosshall *et al.*, 2000). Each glomerulus receives stereotypic input from axon terminals of olfactory sensory neurons (OSNs), which have their cell bodies and dendrites located in the antennae or maxillary palps (Benton *et al.*, 2006; de Bruyne *et al.*, 1999; de Bruyne *et al.*, 2001; Hallem *et al.*, 2004; Shanbhag *et al.*, 1999). All the OSNs innervating a given glomerulus express a typical repertoire of ligand-gated chemoreceptors (Benton *et al.*, 2006; Couto *et al.*, 2005; Fishilevich *et al.*, 2005), which represent a wide range of specifications, binding either a single, few, or many distinct chemicals (Hallem *et al.*, 2006; Hallem *et al.*, 2004; Knaden *et al.*, 2012; Münch *et al.*, 2016; Seki *et al.*, 2017; Wicher *et al.*, 2021).

Most OSNs project bilaterally to the corresponding glomeruli in the left and right AL (Gaudry *et al.*, 2013; Tobin *et al.*, 2017). In the AL, OSNs convey odor signals to excitatory uniglomerular projection neurons (uPNs), which branch only within a single glomerulus, or to inhibitory multiglomerular PNs (mPNs) and inhibitory or excitatory local interneurons (LNs) (Ai *et al.*, 2013; Bates *et al.*, 2020; Cuntz *et al.*, 2007; Kazama *et al.*, 2008; Kazama *et al.*, 2009; Kreher *et al.*, 2008; Masse *et al.*, 2009; Ng *et al.*, 2002; Tanaka *et al.*, 2012; Wilson, 2013). LNs innervate each several glomeruli and are the key modulatory neurons in the AL (Chou *et al.*, 2010; Seki *et al.*, 2010). The highly converging OSNs-to-PN signal transmission (Chen *et al.*, 2005; Jeanne *et al.*, 2015; Masse *et al.*, 2009) is lateralized, activating ipsilateral uPNs more strongly than contralateral ones (Agarwal *et al.*, 2011; Gaudry *et al.*, 2013; Tobin *et al.*, 2017). From the AL, uPNs and mPNs relay processed signal information to higher brain centers (Bates *et al.*, 2020; Fiala, 2007; Galizia, 2014; Guven-Ozkan *et al.*, 2014; Jefferis *et al.*, 2007; Keene *et al.*, 2007; Norgate *et al.*, 2006; Strutz *et al.*, 2014).

The stereotypic activity pattern elicited by distinct odorants encodes the odor space, represented in a so-called odotopic map of the AL according to the glomerular activation by distinct chemical classes. (Couto *et al.*, 2005; Grabe *et al.*, 2018; Grabe *et al.*, 2015; Knaden *et al.*, 2014; Laissue *et al.*, 2008). Some odorants induce a fixed innate behavior (aversion or attraction), activating characteristically specific glomeruli (Gao *et al.*, 2015; Grabe *et al.*, 2018; Knaden *et al.*, 2014; Knaden *et al.*, 2012; Semmelhack *et al.*, 2009). The encoding of hedonic valence already at the level of the AL is important for a fast odor coding. Most odorants are encoded in a combinatorial manner in the fly AL by activating multiple OSNs types expressing broadly tuned

receptors and their glomerular circuits, including broadly tuned uPNs (de Bruyne *et al.*, 2001; Galizia, 2014; Masse *et al.*, 2009; Sachse *et al.*, 2016; Seki *et al.*, 2017; Silbering *et al.*, 2007; Silbering *et al.*, 2008; Szyszka *et al.*, 2015). Certain chemoreceptors and their downstream glomerular circuits, however, have evolved a very high specificity and sensitivity to single or very few chemicals (Andersson *et al.*, 2015; Haverkamp *et al.*, 2018; Keesey *et al.*, 2021). These narrowly tuned glomerular circuits often belong to dedicated olfactory pathways, called "labeled lines", which process information regarding single odorants of particular importance for reproduction and survival (Datta *et al.*, 2008; Dweck *et al.*, 2015; Gao *et al.*, 2015; Kurtovic *et al.*, 2007; Stensmyr *et al.*, 2012). An extreme example is the DA2 glomerulus, which responds exclusively to geosmin, an ecologically relevant chemical that alerts flies to the presence of harmful microbes, causing the fly to avoid laying eggs at these locations (Stensmyr et al., 2012). This dedicated olfactory pathway and its receptor sequence is conserved throughout evolution (Keesey *et al.*, 2021; Keesey *et al.*, 2019). Another example is glomerulus VA1v, which responds to methyl laurate, a pheromone that induces a strongly attractive response in female flies leading to aggregation behavior (Dweck *et al.*, 2015). DL5, on the other hand, is an example of a broadly tuned glomerulus, innervated by OSNs activated by several odorants, like E2-hexenal and benzaldehyde (Knaden *et al.*, 2012; Mohamed *et al.*, 2019b; Münch *et al.*, 2016; Seki *et al.*, 2017). This functional diversity suggests differences in neuronal composition and synaptic connectivity between broadly and narrowly tuned glomeruli.

A survey of neuronal composition across glomeruli revealed great variation in the numbers of the different types of neurons innervating narrowly and broadly tuned glomeruli (Grabe *et al.*, 2016). In general, narrowly tuned glomeruli are innervated by more uPNs and fewer LNs compared to more broadly tuned glomeruli (Chou *et al.*, 2010; Grabe *et al.*, 2016). In addition, narrowly tuned OSNs receive less global LN inhibition than broadly tuned ones (Grabe *et al.*, 2020; Hong *et al.*, 2015; Schlegel *et al.*, 2021). For example, in female flies, the narrowly tuned glomerulus DA2 contains dendrites of 6-8 uPNs, whereas the broadly tuned glomerulus DL5 houses only 1 or 2 uPNs and has a higher number of innervating LNs. Interestingly, both glomeruli are innervated by the same number of OSNs (Grabe *et al.*, 2016).

Little is known, however, about the microarchitecture of the synaptic circuitry in distinct glomeruli and, in particular, about ultrastructural differences between narrowly vs. broadly tuned glomerular circuits. Electron microscopy (EM) allows volume imaging with dense reconstruction of fine neurite branches and synapses in brain tissue at nanometer resolution, necessary to map synapses (Briggman *et al.*, 2006; Cardona *et al.*, 2009; Helmstaedter, 2013; Meinertzhagen, 2018; Rybak, 2013). The first ultrastructural insights into the synaptic connectivity of *Drosophila* olfactory glomeruli were obtained by studies based on serial section transmission EM (ssTEM) (Rybak, 2016; Tobin *et al.*, 2017). Rybak *et al*. (2016) showed that all three basic classes of AL neurons make synapses with each other, while Tobin *et al*. (2017) revealed that the differences in number of innervating uPNs between the left and right DM6 glomeruli are compensated by differences in synaptic strength. With focused ion beam-scanning electron microscopy (FIB-SEM; (Knott *et al.*,

2008)) a complete reconstruction of all neurons in the narrowly tuned, pheromone processing glomerulus VA1v was obtained (Horne *et al.*, 2018). Recent technological innovations in ssTEM, FIB-SEM and automated neuron reconstruction have made connectome datasets of the adult *Drosophila* central nervous system available (Li, P. H. *et al.*, 2020; Saalfeld *et al.*, 2009; Scheffer *et al.*, 2020; Zheng *et al.*, 2018) and provided complete circuit descriptions of several brain centres (Auer *et al.*, 2020; Bates *et al.*, 2020; Coates *et al.*, 2020; Dolan *et al.*, 2019; Felsenberg *et al.*, 2018; Hulse *et al.*, 2021; Huoviala *et al.*, 2020; Li, F. *et al.*, 2020; Marin *et al.*, 2020; Otto *et al.*, 2020; Schlegel *et al.*, 2021).

In an attempt to find answers to how highly specialized olfactory glomerular circuits of dedicated olfactory pathways differ in their signal integration from broadly tuned glomerular circuits, we compared the microarchitecture and synaptic circuitry of a narrowly and a broadly tuned glomerulus (DA2 and DL5). By using a correlative workflow combining transgenic markers with FIB-SEM, in order to identify these glomeruli, we reconstructed OSNs, uPNs and multiglomerular neurons (MGNs), mapped all associated synapses and compared the circuit organization of both glomeruli.

RESULTS

Volume-based electron microscopy of two different olfactory glomeruli

To compare the synaptic circuitries of two olfactory glomeruli known to belong to either narrowly or broadly tuned glomerular types in *Drosophila melanogaster*, we mapped all synapses of glomeruli DA2 (right AL) and DL5 (left AL) in a single female fly (**Figure 1A-B**) with the aid of FIB-SEM. A partial reconstruction of a second DA2 in another fly was used to measure neuronal volume (see Methods). The reconstructions were based on high resolution (4x4x20 nm) datasets (**Figure 1**; **Figure 1 – video 1),** thus allowing reconstruction of the finest neuronal branches (~20 nm diameter; **Figure 1C-D**) as well as mapping chemical synapses (example in **Figure 1E**) in the two volumes of interest (VOI). To restrict the imaging volume to the target VOIs, we employed a correlative approach for the first time for a *Drosophila* EM volume reconstruction. Glomeruli DA2 and DL5 were identified by their size, shape and location in brains of transgenic flies (*Orco-GAL4; UAS-GCaMP6s*) using the glomerular map of (Grabe *et al.*, 2015). The flies expressed the green fluorescent protein GCaMP6 coupled with calmodulin and M13 (a peptide sequence from myosin light-chain kinase; **Figure 1A-B**). Subsequently, the identified glomeruli were marked by laser branding using a two-photon laser (Bishop *et al.*, 2011). These fiducial marks were apparent under both light (Figure 1A-B) and electron microscopy **(Figure 1C-D)** and facilitated the delimitation of the VOIs during FIB-SEM scanning. We produced two complete FIB-SEM datasets: one for glomerulus DA2 and one for DL5 (pure imaging time for both glomeruli: ~60 h) and a partial dataset for DA2 in a second fly.

Skeleton based neuron reconstruction and synapse identification

We reconstructed all neurons within the two VOIs (example neuron: **Figure 1F**) and mapped all their synaptic connections using an iterative skeleton-based reconstruction approach, similar to previously reported procedures (Berck *et al.*, 2016; Schneider-Mizell *et al.*, 2016; Zheng *et al.*, 2017) with the aid of the web-based neuron reconstruction software CATMAID (http://www.catmaid.org; RRID:SCR_006278; (Cardona *et al.*, 2009; Schneider-Mizell *et al.*, 2016); **Figure 1 – video 1**). Synapses were identified by their presynaptic transmitter release site, which in *Drosophila* is composed of a presynaptic density called a T-bar, surrounded by synaptic vesicles and apposed postsynaptic elements (**Figure 1E**), as previously described (Fröhlich, 1985; Huang *et al.*, 2018; Li, P. H. *et al.*, 2020; Rybak *et al.*, 2016; Trujillo-Cenoz, 1969). All synapses observed in our FIB-SEM data sets were polyadic, i.e. each presynaptic site connected to multiple postsynaptic sites (See example in **Figure 1E**), a feature of insect brain synapses (Hartenstein, 2016; Malun *et al.*, 1993; Meinertzhagen *et al.*, 1991; Prokop *et al.*, 2006; Rybak *et al.*, 2016). Some synapses had up to 16 postsynaptic sites (**Figure 2 – figure supplement 1B**), i.e. one T-bar and 16 single synaptic profiles (i.e. sixteen 1:1 single output-input connections). Short neuronal fragments (<10 µm),

which could not be connected to any neuronal fiber were designated as "orphans". These fragments represented 4% of the total length of all traced neuronal fibers in DA2 and 6% in DL5 and contained about ~12% of all synaptic contacts in both glomeruli.

Glomerular neurons: classification, description and inventory

Previous descriptions of the ultrastructural characteristics of the AL in *Drosophila* helped to classify AL neurons into 3 main classes (**Figure 2A**) Olfactory sensory neurons (OSNs), uniglomerular projection neurons (uPNs) and multiglomerular neurons (MGNs; cells that interconnect multiple glomeruli). MGNs are further subdivided into multiglomerular projection neurons (mPNs) and local interneurons (LNs) (Berck *et al.*, 2016; Gruber *et al.*, 2018; Horne *et al.*, 2018; Li, P. H. *et al.*, 2020; Rybak *et al.*, 2016; Schlegel *et al.*, 2021; Zheng *et al.*, 2017). Most of the neuronal profiles within the MGN neuron class belong probably to inhibitory local neurons, as this cell type is the most numerous and broadly arborizing of the multiglomerular cell types in the antennal lobe (Chou *et al.*, 2010; Lin *et al.*, 2012). In addition, we observed a few neuronal fibers with an electron-dense and vesicle-rich cytosol, which we interpreted to be either peptidergic neurons (Eckstein *et al.*, 2020; Nässel *et al.*, 2006) or the contralaterally projecting, serotonin-immunoreactive deutocerebral (CSD) neuron, (Coates *et al.*, 2020; Dacks *et al.*, 2006; Eckstein *et al.*, 2020; Goyal *et al.*, 2013; Zheng *et al.*, 2017). Except for these neuronal fibers containing abundant electron-dense vesicles, all other neuronal fibers were assigned to either OSNs, uPNs or MGNs based on their morphology (**Figure 2A, B;** see Methods).

OSNs formed large, elongated synaptic boutons (**Figure 2A**), had the largest volume/length ratio of all three neuron classes (**Figure 2 – figure supplement 1A**) and displayed the lowest degree of branching intensity of all neurons in both glomeruli (**Figure 2B**). In agreement with what had been observed in other glomeruli (Rybak *et al.*, 2016), the majority of output synapses made by OSN terminals were triads (1:3) and tetrads (1:4). The T-bars of OSN synapses exhibited a large variation in size and some of them were large enough to accommodate 16 postsynaptic contacts (**Figure 2 – figure supplement 1B**)**.** The frequency of large T-bars was much higher in OSNs than in other neuron classes with an average polyadicity (average number of postsynaptic sites at each T-bar) of 6 (1:6; (**Table 1,** row 14). As OSNs had the greatest T-bar and output density along their axons (**Table 1**, row 10-11) they also displayed the largest synaptic ratios (both for the T-bars/input sites and output sites/input sites) of all neuron classes (**Table 1,** row 12-13), which was in line with previous observations (Rybak *et al.*, 2016).

The uPNs exhibited the highest degree of branching intensity of the three neuron classes in both glomeruli (**Figure 2A-B**). They showed numerous very fine apical branches that frequently connected multiple times via spines to the same presynaptic site, leading to an entangled 3D shape typical for this neuron class (**Figure 2A**) (Rybak *et al.*, 2016; Schlegel *et al.*, 2021; Tobin *et al.*, 2017). uPNs had the smallest volume/length ratio of all neuron classes (for the DA2: **Figure 2 - supplement**

1A). In addition to having many fine branches, uPN dendrites also had enlarged regions with almost no cytosol that were packed with large mitochondrial profiles extending over considerable distances. These enlarged profiles showed a larger degree of mitochondria fission (dividing and segregating mitochondrion organelles; personal observation) than the other neuron classes with rather round and compact mitochondria (**Figure 2A**; FIB-SEM image; see data availability). Seven uPNs were found in DA2, confirming light microscopy findings (Grabe *et al.*, 2016). Two of them (PN#1, PN#2; see data availability) branched broadly and innervated the full glomerulus, and received more synaptic input than the other 5 uPNs (PN#3-#7; **see Table S3**), which branched exclusively in sub-regions of the glomerulus, with partial overlap. In addition to abundant clear small vesicles (~20 nm in diameter) (Bates *et al.*, 2020; Strutz *et al.*, 2014; Yasuyama *et al.*, 2003), uPN dendrites also displayed small electron-dense vesicles, as previously reported for PN axon terminals in the mushroom body calyx (Butcher *et al.*, 2012; Yang *et al.*, 2022). These electron-dense vesicles are packed with different types of neuropeptides that act as neuromodulators or co-transmitters (Croset *et al.*, 2018; Eckstein *et al.*, 2020; Gondré-Lewis *et al.*, 2012; Li *et al.*, 2017). In both glomeruli, uPNs had the highest neuronal synaptic input density and the lowest T-bar and output density of the three neuron classes (**Table 1,** row 9-11; DA2 and DL5 differences: see next section). The synaptic ratios (T-bars/input sites and output sites/input sites) were much lower for uPNs than for the other neuron classes (**Table 1,** row 12-13). The majority of uPN dendritic output synapses (feedback synapses) were tetrads in both glomeruli, with an average polyadicity of around 5 (lower than in OSNs; (**Figure 2 – supplement 1; Table 1,** row 14).

The majority of the neuronal fibers in both glomeruli belonged to MGNs (**Figure 2A**). MGNs exhibited variable morphology and ultrastructure, as expected, but shared also some ultrastructural features. Their synaptic boutons were formed by thin fibers, thus the volume/length ratio of MGNs was lower than that of OSNs but greater than that of uPNs (**Figure 2 – figure supplement 1A**). A similar relationship was found for the number of output sites and the T-bar density along MGN fibers, which were smaller than in OSNs but larger than in uPNs (**Table 1,** row 10-11). In contrast, branching intensity in MGNs was larger than in OSNs but smaller than in uPNs (**Figure 2B**). The synaptic ratio of output-to-input sites was around one (**Table 1**, row 12-13). MGNs had the lowest polyadicity (~3) of the three neuron classes (**Table 1**, row 14) and their synapses were mainly triads (**Figure 2 – supplement 1D**). Interestingly, besides the abundant clear small vesicles (~20 nm in diameter), some MGNs had small electron-dense vesicles, most likely housing the neuropeptide sNPF (Nässel *et al.*, 2008).

DA2 is more densely innervated and has a higher synapse density than DL5

In our FIB-SEM datasets the volume of glomerulus DA2 was 45% smaller than that of glomerulus DL5 (1500 μm^3 vs. 2700 μm^3), which is in agreement with measurements based on light microscopy (DA2 = 1600 μm^3, DL5 = 2900 μm^3 (Grabe *et al.*, 2016). We also confirmed that a similar

number of OSNs (44-46 OSNs) innervated both glomeruli (**Figure 2C**), and that each glomerulus received OSN innervation from both the ipsilateral and contralateral antennae (Grabe *et al.*, 2016; Vosshall *et al.*, 2000). Also in agreement with (Grabe *et al.*, 2016), the DA2 glomerulus was innervated by 7 uPNs whereas DL5 had a single uPN (**Figure 2C**). MGN cell numbers could not be counted in our study due to their multiglomerular morphology, which also prevented us from tracing MGN fibers to their soma due to our partial volume acquisition (see Methods).

To investigate differences between DA2 and DL5 we turned our attention to their glomerular innervation and synaptic composition. We measured the total length (sum in µm) of all neuronal fibers of each neuron class within the DA2 and DL5 (**Figure 2C; Table 1**, row 1). In addition, we counted all T-bars and their output sites (1:1 synaptic contacts) as well as all postsynaptic sites (input sites) for all neuron fibers together and for each neuron class individually (**Table 1, row 2-4**). We counted in total ~ 14 000 synaptic contacts and 2648 T-bars in DA2 and ~ 17 000 contacts and 3387 T-bars in DL5 (**Figure 2C, Table 1, row 4**). Most of these synapses were triads and tetrads (**Figure 2 – figure supplement 1B-D**). In order to compare DA2 and DL5 we normalized neuronal length and synaptic numbers to glomerular volume. We then analyzed (**1**) the innervation density, i.e., the length of neuronal fibers per glomerular volume (µm/µm^3) and (**2**) the glomerular synaptic density (T-bar #, output site or input site #/µm^3). Data are reported in total for all neuronal fibers of each neuron class (**Table 1, row 5-8**) and as an average for neuronal fibers of the respective neuron class **(Figure 3)**. In addition, we compared (**3**) the average polyadicity for each neuron class **(Figure 3)** and **(4)** the average neuronal synaptic density (T-bar, output and input site density along each neuronal fiber) (#/µm) (**Figure 3 – figure supplement 1B**).

We observed that the average neuron innervation density of OSNs was 20% higher in DA2 than in DL5 (**Figure 3A**), **Table S1**). Also the glomerular synaptic density of input sites, output sites and T-bars along OSNs was significantly higher in DA2 than in DL5 (**Figure 3A**). OSNs in DA2 formed therefore more input sites, and much more T-bars and output sites per glomerular volume than in DL5 (**Table 1**, row 7-8; relative differences: **Table S1**). In contrast, the density of input sites distributed along the length of OSN fibers was similar in DA2 and DL5, whereas T-bar and output site density along the OSN axons was significantly higher in DA2 (**Figure 3 – figure supplement 1A**).

We then asked if the DA2 glomerulus, due to its higher number of uPNs, also had a higher uPN innervation density and synaptic density of its postsynaptic sites and/or presynaptic sites compared to the DL5 glomerulus, which contains a single uPN. In the DA2, the fibers of the 7 uPNs had almost the same total length as the fibers of the single uPN in the more voluminous DL5 (4652 µm in DA2 vs. 5015 µm in DL5; **Table 1**, row 1). The DA2 uPNs had in addition a similar total number of input sites than the single uPN in DL5 (3887 vs. 3955; **Table 1**, row 2). As such, in DA2 the total innervation density of its 7 uPNs was higher as compared to the innervation density of the single uPN in DL5 (**Table 1**, row 5), even though the average innervation density of DA2-uPNs was lower (**Figure 3B**). The total glomerular input density of all uPNs was higher in DA2 as compared to DL5

(**Table 1**, row 6). On the other hand, the total glomerular synaptic density of the T-bars and output sites was similar in DA2 and DL5 (**Table 1**, rows 7-8). In line with these results, the neuronal density of T-bars and output sites was less in the DA2 uPNs compared to the DL5 single uPN, whereas the neuronal density of input sites was similar (**Figure 3 – figure supplement 1B; Table 1**, row 9-10). This caused almost twice as high synaptic ratios (T-bars-to-inputs and outputs-to-inputs) in the DL5 uPN relative to DA2 uPNs (**Table 1**; row 12-13).

We then hypothesized that DA2 will have a lower innervation density of MGNs (mainly LNs) than DL5 as it had been reported that DL5 is innervated by fewer LNs (Chou *et al.*, 2010; Grabe *et al.*, 2016). However, we observed the opposite: the innervation density of MGNs was significantly higher in DA2 than in DL5 (**Figure 3C**), with slightly higher total innervation density (**Table 1,** row 5**).** Interestingly, only the glomerular input density was significantly higher for DA2 MGNs compared to that found in DL5, not the glomerular synaptic density of output sites or of the T-bars (**Figure 3C**). However, the total glomerular synaptic density of input sites, output sites and T-bars were still higher in DA2 than in DL5 **(Table 1,** rows 6-8**).** Synaptic densities along the MGN fibers were similar in DA2 and DL5 (**Figure 3 – supplement 1**).

In summary, the DA2 glomerulus is more densely innervated than DL5 and has a more densely packed neuropil with more synaptic contacts relative to the DL5. The DA2 has a significantly higher innervation density and higher density of T-bars, output and input sites per volume (**Figure 3D**, **Table 1,** row 5-8**).** The degree of synapse polyadicity is also significantly higher in DA2 than in DL5 (**Figure 3D, Table 1,** row 14) due to a shift to higher polyadicity among OSN (**Figure 3A**) and MGN synapses (**Figure 3C**). OSNs show the strongest shift in polyadicity, with tetrads being the most abundant synapse type in DA2 whereas triads are the most abundant in DL5 OSNs (**Figure 2 – figure supplement 1B).**

Lateralization of OSN glomerular connectivity

In *Drosophila melanogaster*, the majority of olfactory glomeruli receive bilateral OSN input (Silbering *et al.*, 2011; Stocker *et al.*, 1990; Stocker *et al.*, 1983; Vosshall *et al.*, 2000) see scheme in **Figure 4A**). Recent studies have shown that ipsi- and contralateral OSNs are asymmetric in their synaptic connectivity to other neurons in the majority of the glomeruli (Schlegel *et al.*, 2021; Tobin *et al.*, 2017) and that ipsi- and contralateral OSNs activate uPNs in an asymmetric way (Gaudry *et al.*, 2013; Tobin *et al.*, 2017). However, not all glomeruli appear to have the same degree of lateralized OSN connectivity (Schlegel *et al.*, 2021). At least for one narrowly tuned glomerulus (DA1), there is functional evidence that in female flies its uPNs are evenly activated by either ipsi- or contralateral antennal stimulation (Agarwal *et al.*, 2011). We hypothesized that this lack of lateralization could be a feature of other narrowly tuned glomeruli.

Ipsi- and contralateral OSNs in DA2 and DL5 were identified based on the location and trajectory of their axons (**Figure 4B**). In both glomeruli, ipsilateral OSN terminals were longer than

their contralateral counterparts within the VOI, while polyadicity was stronger in contralateral axons. Synaptic density was not consistently higher or lower in ipsilateral OSNs compared to contralateral ones in DA2 and DL5 (**Figure 4 – figure supplement 1**).

We observed that the synaptic output of ipsi- vs. contralateral OSNs was asymmetric, with significant differences in the ipsi- and contralateral OSN output to either uPNs, OSNs or MGNs (**Figure 4C**, DA2 and DL5). In agreement with previous observations in other glomeruli (Schlegel *et al.*, 2021), the output fraction to uPNs and OSNs was greater in ipsilateral OSNs than in contralateral ones (**Figure 4C**, DA2 and DL5). Vice versa, the OSN output to MGNs was greater in the contralateral glomerulus than in the ipsilateral side (**Figure 4C**, DA2 and DL5). However, the differences between the medians and means were smaller in DA2 than in DL5 (**Figure 4C**; differences between means: see data availability).

Our finding of less lateralized connections in the DA2 (**Figure 4C**, DA2 and DL5) was also observed in another narrowly tuned glomerulus (VA1v; Dweck et al., 2015) for which connectome data is available (Horne *et al.*, 2018). In VA1v, the OSN output to uPNs and MGNs was significantly asymmetric in the same manner as in DA2 and DL5, i.e. with greater ipsilateral OSN output fractions to uPNs and OSNs and greater contralateral OSN output fraction to MGNs (**Figure 4C**). Asymmetry in the VA1v OSN output fractions was even less distinct than in DA2 (regarding both the difference between the median and the mean; **Figure 4C** and data availability). In VA1v, the OSN output fraction to OSNs was similar in ipsi- and contralateral OSNs (**Figure 4C**). In addition, the OSN input, from either sister OSNs or MGNs, was asymmetric in DL5 but not in the narrowly tuned glomeruli (**Figure 4D**). The inputs from uPNs to ipsi- or contralateral OSNs were not compared due to their low numbers.

In summary, our data add to the knowledge of lateralized connectivity within olfactory glomeruli and supports the hypothesis that narrowly tuned glomeruli have a lower degree of lateralization of OSN connectivity compared to broadly tuned glomeruli.

Glomeruli DA2 and DL5 differ in several features of their circuitry

Next, we asked whether the synaptic circuitries of DA2 and DL5 differ from each other. We counted each synaptic contact (**Table S2 and S3**) and categorized the distinct connection motifs according to the neuron class to which the output and input neuron belonged (**Figure 5A; Table S2).** Each connection motif (for example OSN>uPN, i.e., the OSN-to-uPN feedforward connection) was then assessed for its relative synaptic strength, i.e. how many synaptic contacts of this particular connection motif were found compared to the total number of synaptic contacts within the respective circuitry (**Figure 5A-D**; see Methods).

We found that neurons from each class made synaptic contacts with each other in DA2 and DL5, as previously reported for other glomeruli (Berck *et al.*, 2016; Horne *et al.*, 2018; Rybak *et al.*, 2016; Schlegel *et al.*, 2021; Tobin *et al.*, 2017). In both DA2 and DL5, OSNs provided the strongest

relative synaptic output, i.e. 49% of all synaptic connections in DA2 and 43% in DL5 were formed by OSNs (**Figure 5B-C**). Thus, even though DA2 and DL5 had similar numbers of OSNs (44 and 46, respectively), those in DA2 provided a stronger circuit output (14% stronger; **Table S2**) than those in DL5 (**Figure 5B-C)**. In both glomeruli the main OSN output partners were MGNs and uPNs, i.e. 27% of all circuitry connections in DA2 and 24% in DL5 were OSN>MGN connections and 20% in DA2 and 18% in DL5 were OSN>uPN connections (**Figure 5B-C**). In DA2, interestingly, each of the 7 uPNs received input from almost all OSNs and so could maintain a high degree of convergent signal transmission (**Table S3**). In contrast, OSNs received the lowest relative input of all neuron classes in DA2 and DL5 (7% and 8% respectively; **Figure 5B-C**). In line with previous observations in other glomeruli (Horne *et al.*, 2018; Schlegel *et al.*, 2021), OSNs also made abundant axo-axonic synapses with sister OSNs (2.6% in DA2 and 1.5% in DL5; **Figure 5B-C**). Thus, the relative synaptic strength of the OSN>OSN connection was 70% stronger in DA2 than in DL5 (**Figure 5B-C; Table S2**).

The uPNs in both glomeruli had the weakest relative output of all neuron classes within their circuitry, and this was even weaker (38%) in DA2 (**Figure 5B-C; Table S2**). In contrast, the relative synaptic input onto uPNs was greater in DA2 than in DL5 (33% vs. 28%, respectively; **Figure 5B-C;** 16% stronger in DA2; **Table S2**), which is in line with our finding that in DA2, the uPNs provide more input sites per unit of glomerular volume than in the DL5 (**Figure 3B-C**). In both glomeruli, the feedback connections from uPNs (depicted in **Figure 5A**), were almost exclusively directed towards MGNs, as previously reported for the broadly tuned DM6 and the narrowly tuned glomerulus VA1v (Horne *et al.*, 2018; Tobin *et al.*, 2017). However, the relative synaptic strength of the uPN>MGN connection was 40% weaker in DA2 than in DL5 (uPN>MGN: 10% in DA2 and 17% in DL5). Only a few cases of uPN>OSN synaptic connections were observed (a total of 16 in DA2 and 26 in DL5) representing a synaptic strength of 0.1% in DA2 and 0.2% in DL5 (**Table S2**). Finally, uPNs in DA2 also made 71 reciprocal synaptic connections (representing a synaptic strength of 0.6%; **Table S2**; **Figure 5B**), consistent with electrophysiological evidence for reciprocal synaptic interactions between sister uPNs (Kazama *et al.*, 2009). The single uPN of the DL5 had 54 dendro-dendritic synapses (representing 0.4% of all DL5 synaptic contacts; **Figure 5C**), which were exclusively autapses, i.e. synapses formed by a neuron onto itself. Dendritic uPN autapses exist also in DA2-uPNs, but they were few: we observed only 14 autaptic uPN-uPN connections in DA2, which were mainly located at the two longest uPN dendrites (for further analysis of autapses see next section).

MGNs received the strongest input in both glomeruli (60% of the total input in DA2 and 64% in DL5; **Figure 5B-C**). This is in line with the observation that MGNs provided the majority of all traced neuronal fibers in each glomerulus and had the highest innervation density of all neuron classes; **Table 1**). The relative output strength of MGNs was similar in both glomerular circuits (~40% of the total output in each glomerulus; **Figure 5B-C**). MGNs made many reciprocal synapses to each other, accounting for 23% of all synapses in both glomeruli (**Figure 5B-C)**. The relative synaptic strength between MGN>uPN was stronger in DA2 (12%) than DL5 (10%) (**Figure 5B-C**;

Table S2). The MGN>OSN feedback connection was relatively weak in both glomeruli (5% in DA2 vs. 6% in DL5; **Figure 5B-C**) but weaker (25%) in DA2 than in DL5 (**Table S2**).

We then looked at the fractional output and input of each neuron class (Figure 5E', E''). In both glomeruli OSNs had a similar proportion of their synaptic output onto uPNs (40%-41%), onto MGNs (55% in both) and onto sister OSNs (4%-5%) (**Figure 5E'**). From the uPNs perspective, over 93%-96% of their recurrent synaptic output was directed to MGNs in both DA2 and DL5, and few synapses were directed onto OSNs (~1% of the uPN output; **Figure 5E'**). The uPN>uPN output fraction of the 7 uPNs in DA2 (reciprocal synapses) was twice the uPN output fraction (autaptic) of the single uPN dendrite in DL5 (6% vs. 3%; **Figure 5E'**). MGNs formed synaptic output mainly to other MGNs (58%-59% of the total MGN output in DA2 and DL5). Among MGNs we found also rare cases of autapses. The MGN>uPN output fraction was greater in DA2 (30%) than in DL5 (25%), whereas the MGN>OSN output fraction was smaller in DA2 (12%) than in DL5 (16%; **Figure 5E'**).

Turning to the input fractions of each neuron class, we found that in both glomeruli, OSNs received most of their input from MGNs (>50%). In DA2 the input fraction onto OSNs (MGN>OSN) was smaller than in DL5 (63% vs. 78%; **Figure 5E''**). In contrast, the OSN input fraction from sister OSNs was greater in DA2 (35% vs. 20%; **Figure 5E''**). In both glomeruli, the OSNs received only weak uPN input (2%) (**Figure 5E''**). The input fractions onto the 7 uPNs, formed by uPNs, MGNs and OSNs, in the DA2 and the single uPN in DL5 were similar (**Figure 5E''**). Most uPN input was delivered by OSNs (~62% in both glomeruli) and less from MGNs (~36%). The uPN input fraction from other uPNs in DA2 or the autaptic input from the single uPN in DL5 was small (2%; **Figure 5E''**). In DA2 the MGNs received a smaller fraction of uPN feedback input than in DL5 (17% vs. 26%; **Figure 5E''**) but a greater OSN input fraction (45% vs. 38%; **Figure 5E''**). The fraction of MGN>MGN input was similar in both glomeruli.

To further explore whether the differences in circuitry between DA2 and DL5 reported here might represent features characteristic of narrowly tuned glomeruli, we analyzed connectome data from another narrowly tuned glomerulus (VA1v; (Horne *et al.*, 2018). We calculated the relative synaptic strength between OSNs (n=107), uPNs (n=5) and MGNs (n=74) in the VA1v (**Figure 5D; Table S2**). We found that the two narrowly tuned glomeruli shared five circuit features that were different from the broadly tuned glomerulus DL5: (**1**), OSNs in VA1v, as reported above for DA2, displayed a stronger relative feedforward output to uPNs (22%) and to MGNs (32%) (**Figure 5D**). The uPNs and MGNs in VA1v, received a larger fraction of OSN input than in DL5 (**Figure 5E''**). (**2**), the OSN>OSN synaptic output was four times stronger (6%) than in DL5 (1.5%; **Figure 5B-D, Table S1**). This was also reflected in the OSN output fraction to sister OSNs (10%), which in VA1v was more than twice that of DL5 (4%; **Figure 5E'**) and in the much greater OSN input fraction (38%) to OSNs in the VA1v than in DL5 (20%; **Figure 5E''**). (**3**), in the VA1v the uPN>uPN relative synaptic output was more than twice that of DL5 (1% vs. 0.4% in DL5; **Figure 5D**), which is in accordance with a much greater uPN output fraction to uPNs (14%) in VA1v than in DL5 (3%) (**Figure 5E'**). (**4**), as observed before in DA2, VA1v uPNs had fewer feedback synapses onto MGNs than in DL5

(relative synaptic strength of uPN>MGN connection: 6% vs. 17%; **Figure 5C-D**), also reflected in a smaller output fraction from uPNs to MGNs in VA1v than in DL5 (81% vs. 96%; **Figure 5E'**). In agreement, the MGN input fraction from uPNs in VA1v was much smaller than in DL5 (10% vs. 26%; **Figure 5E''**). (**5**), OSNs in VA1v received a smaller MGN input fraction than DL5 OSNs (60% vs. 78%; **Figure 5E''**).

Besides relative differences (stronger or weaker) in DA2 and VA1v connection motifs compared to DL5, two connection motifs were stronger in DA2 and DL5 than in VA1v: **(1)** the MGN>uPN connection showed a synaptic strength of 12% and 10% in DA2 and DL5 vs. 8% in VA1v (**Figure 5B-D, Table S2**). In agreement with this, the MGN output fraction to uPNs (**Figure 5E'**, MGN output) and the MGN input fraction in uPNs was greater in DA2 and DL5 than in VA1v (**Figure 5E''**, uPN input). **(2)**, the relative synaptic strength in MGN>MGN motifs was similar between DA2 and DL5 (23%; **Figure 5B-C**), but weaker in VA1v (17%; **Figure 5D, Table S2**)**.** This was also reflected in a smaller MGN output and input fraction from or to MGNs (**Figure 5E' and E''**).

In summary, the two narrowly tuned glomerular circuits studied here shared five circuit features when compared with the broadly tuned glomerular circuit (all glomerular circuit features in DA2, DL5 and VA1v are shown in **Figure 6A**). These features were (1) a stronger OSN>uPN and OSN>MGN connection, (2) a much stronger axo-axonic communication between sister OSNs, (3) a stronger dendro-dendritic connection between uPN dendrites, (4) less feedback from uPNs to MGNs and (5) less feedback from MGNs to OSNs (**Figure 6B**).

Autapses in the large DL5 uPN connect distant regions of its dendritic tree

Autapses (synapses made by a neuron upon itself) have seldomly been reported in the *Drosophila* central nervous system (Horne *et al.*, 2018; Takemura *et al.*, 2015). In the DA2 glomerulus we found few autapses in uPNs and MGNs (**Figure 5C; Figure 7A**). In the dendritic tree of the single DL5 uPN, on the other hand, three observers registered 54 autaptic connections independently (see Methods). This represents 3% of the output connections of this neuron and 0.4% of all synaptic contacts in the whole glomerulus (**Figure 7A**; **Figure 5C; E'**). We found that these autapses were not distributed evenly along the dendritic tree of the DL5 uPN. Some dendritic branches received several autaptic inputs, whereas other had no autaptic input (**Figure 7A**) and we hypothesized that these autapses could connect distant parts of this very large dendritic tree. We thus analyzed the exact location and distribution of their presynaptic and postsynaptic sites (**Figure 7A**) We discovered a difference in the distribution of the pre- and postsynaptic elements of DL5 autapses. Whilst their presynaptic T-bars were evenly distributed at basal (strahler order: 5) and distal regions (strahler order: 1-4), 95% of their postsynaptic sites were located in the most distal region (strahler order 2-1; **Figure 7B-C**). We also calculated the geodesic distance (i.e., along-the-arbor distance) from pre- and post-synaptic sites to the basal root node, which is the node point where the uPN enters the glomerulus and is equivalent to the closest point to the soma in our

464 reconstruction. The geodesic distance to the basal root node from the presynaptic site was
465 significantly shorter than for postsynaptic sites (**Figure 7 – figure supplement 1B**). The pre- and
466 postsynaptic sites of each autapse were either close to each other along the dendritic tree, or
467 distant from each other (see examples in the dendrogram depicted in **Figure 7D**). Thus, the
468 geodesic distance between pre- and postsynaptic sites, (see scheme in **Figure 7E**), as well as the
469 number of branching points between pre- and postsynaptic partners, were bimodally distributed
470 (**Figure 7F-G**). Autapses that connected distant dendritic branches were more frequent than those
471 that connected close dendritic branches (**Figure 7E-G**). In summary, we found abundant autapses
472 within the uPN dendrite of DL5 and they were unevenly distributed, with many output sites located
473 in a few sub-branches connecting distal dendritic regions.

DISCUSSION

We hypothesized that specialized, narrowly tuned olfactory glomeruli differ in their ultrastructure and microcircuitry from broadly tuned glomeruli. By comparing data obtained with dense reconstructions of two narrowly tuned olfactory glomeruli with that of a broadly tuned glomerulus in *Drosophila melanogaster,* we found prominent features of narrowly tuned glomeruli involving synaptic composition, lateralization of sensory input and synaptic circuitry.

Glomerular circuit analysis: a correlative approach

The small size of olfactory glomeruli in *Drosophila* gave us the opportunity to reconstruct and analyze the dense connectome of entire glomeruli with volume-based electron microscopy in a reasonable time period. Here we developed a correlative workflow that combines transgenic neuron labeling with near-infra-red-laser-branding for precise volume targeting. We then used FIB-SEM (Bishop *et al.*, 2011) to resolve glomerular networks at the synaptic level. A similar procedure was used recently to investigate single cellular organelles (Ronchi *et al.*, 2021). An advantage of this approach is that it facilitates localization of the volume of interest with high precision and consequently limits to a minimum the volume to be scanned and reconstructed. At the same time, the limitation in volume is a drawback of our workflow, as it was impossible to reconstruct neurons back to their soma. This fact prevented the identification of individual neurons as in other connectome studies (Bates *et al.*, 2020; Berck *et al.*, 2016; Eichler *et al.*, 2017; Horne *et al.*, 2018; Scheffer *et al.*, 2020; Schlegel *et al.*, 2021; Xu *et al.*, 2020; Zheng *et al.*, 2018).

We provide data on innervation and synapse density of olfactory sensory neurons (OSNs), uniglomerular projection neurons (uPNs) and multiglomerular neurons (MGNs) in the *Drosophila* antennal lobe (AL). We observed a higher innervation density of all neuron types but mainly by uPNs and MGNs and in parallel higher density of synaptic contacts along OSN terminals in the narrowly tuned DA2 compared with DL5. These results suggest that narrowly tuned glomeruli have a more densely packed neuropil, with more numerous synaptic connections in the feedforward motifs OSN>uPN and OSN>MGN. Overall, our observations on synapse density were comparable with previous reports (Horne *et al.*, 2018; Mosca *et al.*, 2014; Rybak *et al.*, 2016).

Specific features of narrowly tuned glomerular circuits

Our analysis revealed circuit features in the narrowly tuned glomerulus DA2 and VA1v that might be adaptations specific of such dedicated glomerular circuits. Nevertheless, future studies, analyzing precise numbers of synaptic connections in more individuals, combined with physiological studies and computational models are required to test this hypothesis.

The OSN>uPN feedforward connection is stronger in narrowly tuned glomeruli

Presynaptic OSN terminals provide the major input to uPNs in insect olfactory glomeruli (Chen *et al.*, 2005; Hansson *et al.*, 2000; Horne *et al.*, 2018; Kazama *et al.*, 2008; Lei *et al.*, 2010; Rybak *et al.*, 2018; Schlegel *et al.*, 2021; Tobin *et al.*, 2017). Here we showed that this connection is stronger in DA2 and VA1v than in DL5 (**Figure 5 and 6**). A strong OSNs>uPN synaptic connection will drive non-linear signal amplification, which improves signal detection at low odor concentrations (Bhandawat *et al.*, 2007; Kazama *et al.*, 2008; Masse *et al.*, 2009; Ng *et al.*, 2002). A larger number of synapses of this type could be an adaptation to improve this amplification effect, as shown by artificial increase of synaptic sites in the AL (Acebes *et al.*, 2001) and in lateral horn dendrites (Liu *et al.*, 2022).

Each of the 7 uPNs in DA2 received convergent synaptic input from almost all DA2-OSNs. This is in agreement with reports on the narrowly tuned glomeruli DA1 and VA1v (Agarwal *et al.*, 2011; Horne *et al.*, 2018; Jeanne *et al.*, 2015) and for broadly tuned glomeruli (Chen *et al.*, 2005; Kazama *et al.*, 2009; Masse *et al.*, 2009; Tobin *et al.*, 2017; Vosshall *et al.*, 2000). High OSN>uPN convergence is the main driver of highly correlated activity among uPNs in pheromone coding glomeruli in flies as well as moths (Kazama *et al.*, 2009; Rospars *et al.*, 2014). High convergence in the lateral horn improves signal transmission from uPNs to lateral horn neurons without sacrificing speed (Huoviala *et al.*, 2020; Jeanne *et al.*, 2015). In the mushroom body calyces, however, the high degree of convergence is only pursued for DA2 uPNs, which converge onto few Kenyon cells, whereas VA1v uPNs synapse randomly onto many dispersed Kenyon cells (Caron 2013; Zheng 2020; Li 2020), indicating diverse signal integration in the mushroom body.

From our study, we hypothesize that in narrowly tuned glomerular circuits, which have more uPNs, the maintained strong OSN>uPN convergence, improve signal transmission accuracy. Secondly, a stronger OSN>uPN connection might compensate for the lack of OSN>uPN signal transmission sites in the case of odorants activating OSNs in a single glomerulus.

Reciprocal connections between sister OSNs and sister uPNs are stronger in narrowly tuned glomeruli

The reciprocal OSN-OSN synapse is generally stronger in narrowly tuned glomeruli DA1, DL3 and DL4, compared to broadly tuned glomeruli DL5, DM6, DM3 and DM4 (Dweck *et al.*, 2015; Ebrahim *et al.*, 2015; Grabe *et al.*, 2016; Knaden *et al.*, 2012; Schlegel *et al.*, 2021; Seki *et al.*, 2017; Suh *et al.*, 2004; Tobin *et al.*, 2017). A high degree of axo-axonic synapses between sister OSNs was also found in VA1v (Horne *et al.*, 2018; Schlegel *et al.*, 2021)and DA2 but not in the DL5 (this study). Hence, we suggest that a strong OSN-OSN connection is a characteristic feature of the synaptic circuitry of narrowly tuned olfactory glomeruli. Axo-axonic connections have also been reported between gustatory and mechanosensory neurons in *Drosophila* larvae (Miroschnikow *et al.*, 2018) and in the olfactory epithelium and the olfactory bulb of vertebrates (Hirata, 1964; Shepherd *et*

al., 2021). In vertebrates, axo-axonic synapses between excitatory sensory neurons are involved in correlated transmitter release (Cover *et al.*, 2021), reminiscent of correlated uPN activity due to reciprocal synaptic and electric coupling in the *Drosophila* AL and LH (Huoviala *et al.*, 2020; Kazama *et al.*, 2009). A strong OSN-OSN connection also has the potential to increase the correlation of OSN spiking events and therefore facilitate a robust OSN signal (de la Rocha *et al.*, 2007).

Reciprocal dendro-dendritic synapses between sister uPNs are reported here for the DA2 have been reported previously also for glomeruli DM6, DM4, VA7 and VA1v (Horne *et al.*, 2018; Kazama *et al.*, 2009; Rybak *et al.*, 2016; Tobin *et al.*, 2017). These types of synapses enhance uPN signal correlation (Kazama *et al.*, 2009), as reported for mitral and tufted cells of the vertebrate olfactory bulb, the circuit equivalent to PNs of insect ALs (Christie *et al.*, 2005; McTavish *et al.*, 2012; Shepherd *et al.*, 2021). In *Drosophila* multiple uPNs could induce correlated PN depolarization events, which improve the signal-to-noise-ratio of PN signal transmission (Chen *et al.*, 2005; Jeanne *et al.*, 2015; Kazama *et al.*, 2009).

In summary, our data give evidence that reciprocal OSN-OSN and uPN-uPN connections are a prominent feature of the synaptic circuit of narrowly tuned glomeruli. We suggest that those reciprocal OSN-OSN and uPN-uPN connections support correlation of neuronal activity and therefore boosts signal induced depolarization events. This will in turn enhance the signal-to-noise ratio (accuracy) and transmission probability of weak and/or irregular odorant input, increasing processing speed.

Less lateralization in the OSN bilateral connectivity in narrowly tuned glomeruli

In *Drosophila*, most OSN axons project bilaterally and form synapses in their corresponding glomerulus on both the left and right brain hemispheres (Couto *et al.*, 2005; Kazama *et al.*, 2009; Schlegel *et al.*, 2021; Silbering *et al.*, 2011; Stocker *et al.*, 1990; Tobin *et al.*, 2017; Vosshall *et al.*, 2000). This is rarely observed in other insects and absent in vertebrates (Anton *et al.*, 2003; Dalal *et al.*, 2020; Galizia *et al.*, 1998; Hansson *et al.*, 2000; Masson *et al.*, 1990; Parthasarathy *et al.*, 2013; Stocker *et al.*, 1983). In the mammalian olfactory system, bilateral comparison of olfactory input only occurs in higher brain centers (Dalal *et al.*, 2020). In flies, bilateral sensory input enables them to discriminate odor sources of different spatial origin through bilateral comparison of olfactory stimulation (Borst *et al.*, 1982; Duistermars *et al.*, 2009; Gaudry *et al.*, 2013; Mohamed *et al.*, 2019a; Taisz *et al.*, 2022). Asymmetric OSN connectivity, shown for many olfactory OSNs (Schlegel *et al.*, 2021; Tobin *et al.*, 2017) seems to be the origin of a bilateral contrast in the uPN response (Agarwal *et al.*, 2011; Gaudry *et al.*, 2013; Taisz *et al.*, 2022; Tobin *et al.*, 2017), and is most likely the key to precise odor source localization (Taisz *et al.*, 2022). Bilateral comparison is also used in the lateral horn (a higher olfactory brain center in *Drosophila*) for odorant position coding (Mohamed *et al.*, 2019a). However, not all glomeruli are similar in the magnitude of bilateral asymmetry with respect to their OSN connectivity (Schlegel *et al.*, 2021) or their uPN responses (Agarwal *et al.*, 2011).

In agreement with observations in other olfactory glomeruli (Schlegel *et al.*, 2021; Tobin *et al.*, 2017), we found that glomeruli DL5, DA2 and VA1v (data from: (Horne *et al.*, 2018) have ipsilaterally asymmetric OSN synaptic output to excitatory uPNs and sister OSNs and contralaterally an enhanced OSN>MGN output (**Figure 4**). We believe that, in agreement with a recent study, these asymmetric connections determine a strong left-right-contrast in the uPN response, akin to a "winner-takes-all" principle (Taisz *et al.*, 2022).

We also observed that the degree of bilateral OSN asymmetry in DA2 and VA1v was much weaker than in DL5 (**Figure 4**). Weakly lateralized OSN connectivity is perhaps insufficient to induce an adequate bilateral contrast necessary for odor source localization. Recent work supports this idea by showing the importance of the interplay of asymmetric OSN signaling and LN inhibition to enhance the bilateral contrast of uPN activity and to facilitate navigation (Taisz *et al.*, 2022).

Why do these narrowly tuned glomeruli have weaker bilateral contrast than broadly tuned glomeruli? The answer could lie in the ecological significance of the individual odorants. Geosmin, encoded by glomerulus DA2 (Stensmyr *et al.*, 2012), and the pheromone methyl laurate, encoded by glomerulus VA1v (Dweck *et al.*, 2015), act at short distances, mainly when the fly is walking and not flying. Perhaps, the behavioral response to geosmin or methyl laurate does not need a precise odor source location. On the other hand, food odor detection at a distance, which happens mainly at flying conditions, needs continuous processing of odor position and body alignment to navigate towards the odor source (Demir *et al.*, 2020; Thoma *et al.*, 2015). The bilateral OSN projection onto uPNs in DA2 and VA1v potentially has a distinct function other than odor position coding and could, via the enhancement of the effect of convergence of OSN>uPN signal transmission, enhance odor signal amplification (Bhandawat *et al.*, 2007; Jeanne *et al.*, 2015; Kazama *et al.*, 2009; Masse *et al.*, 2009)

Distinct synaptic integration of local modulatory neurons in narrowly tuned glomeruli

MGNs are composed of multiglomerular projection neurons (mPNs) that project directly to the LH (Bates *et al.*, 2020; Jefferis *et al.*, 2007; Strutz *et al.*, 2014) and inhibitory and excitatory local interneurons (LNs) that interconnect the AL glomeruli (Chou *et al.*, 2010; Liu *et al.*, 2013; Masse *et al.*, 2009; Okada *et al.*, 2009; Seki *et al.*, 2010). Since LNs are the most numerous and broadly arborizing of the multiglomerular cell types in the AL (Chou *et al.*, 2010; Lin *et al.*, 2012), we focus our discussion on these. Multiglomerular LNs are crucial for the modulation of the OSN>uPN signal transmission (Chou *et al.*, 2010; Galizia, 2014; Masse *et al.*, 2009; Seki *et al.*, 2010; Szyszka *et al.*, 2015).

Previous observations have shown that glomeruli DA2 and VA1v have a lower number of innervating LNs (Chou *et al.*, 2010; Grabe *et al.*, 2016) and receive less global interglomerular LN inhibition than broadly tuned glomeruli (Hong *et al.*, 2015). We therefore assumed that DA2 or VA1v would have a lower LN innervation density and less LN synaptic integration in their circuitry. However, we did not observe a general lower synaptic integration in DA2 **(Figure 5**) and found a

618 greater MGN innervation density, and a higher density of input sites than in DL5. VA1v MGNs on
619 the other hand received less synaptic input and provided less output in its glomerular circuit than
620 MGNs in DL5.
621 Taking a closer look at particular synaptic connection motifs of MGNs we saw that narrowly
622 tuned glomeruli had a relatively weak uPN>MGN feedback (**Figure 6**). uPN feedback onto LNs and
623 their reciprocal connection (LN>uPN) were reported in *Drosophila* and other insects, such as honey
624 bees, cockroaches and moths, but their function is still poorly understood (Boeckh *et al.*, 1993;
625 Sachse *et al.*, 2002; Sun *et al.*, 1997). In the honey bee reciprocal dendro-dendritic synapses
626 between excitatory and inhibitory neurons enhance signal contrast and the reliability of true signal
627 representations throughout the AL (Sachse *et al.*, 2002; Yokoi *et al.*, 1995). Here we could not
628 differentiate the LN types involved in the uPN>MGN synaptic motif. However, the prevailing
629 uPN>LN synapses involve mainly widespread pan-glomerular LNs in the adult (Horne et al., 2018)
630 and larval AL (Berck et al., 2016), which are important for combinatorial coding (Galizia, 2014;
631 Sachse *et al.*, 2016). Thus, weaker uPN>MGN feedback in the narrowly tuned DA2 and VA1v circuits
632 might be a compensatory mechanism to lower the computational demand of interglomerular
633 communication for odor identity coding.
634 We also observed that OSNs received less MGN in the narrowly tuned DA2 and VA1v than
635 in the DL5, suggesting that the OSNs in DA2 and VA1v receive relatively weak presynaptic
636 inhibition. Pan-glomerular GABAergic LNs induce presynaptic inhibition at OSN presynaptic site
637 (Berck *et al.*, 2016; Schlegel *et al.*, 2021). These inhibitory LNs are drivers of balanced glomerular
638 gain control and are a key player for odor identity coding, balancing incoming and alternating odor
639 intensities (Asahina *et al.*, 2009; Galizia, 2014; Hong *et al.*, 2015; Olsen *et al.*, 2008; Root *et al.*,
640 2008; Sachse *et al.*, 2016; Silbering *et al.*, 2008; Szyszka *et al.*, 2015; Wang, 2012). Our data support
641 these observations and provide an argument for why narrowly tuned OSNs receive much lower
642 inhibition during AL stimulation with odorants activating other OSN populations (Hong *et al.*, 2015).
643 Even though DA2 and VA1v might receive less interglomerular inhibition, their OSN>MGN output
644 is still strong, in agreement with studies showing that throughout the AL, global lateral inhibition
645 mediated by LNs scales with general OSN activation (Hong *et al.*, 2015; Olsen *et al.*, 2008).
646 In summary, narrowly tuned circuits are probably influenced more strongly by
647 intraglomerular than by interglomerular modulation. Narrowly tuned circuits perhaps have greater
648 computational capacities in intraglomerular modulation of signal transmission, which could be
649 important for example for PN fine-tuning and response adjustment (Assisi *et al.*, 2012; Ng *et al.*,
650 2002).
651 Above we discussed putative generic features of narrowly tuned glomerular circuits.
652 Besides these circuit features, we found a strong MGN>MGN connection in the aversive glomerular
653 circuits DA2 and DL5 in contrast to a much weaker MGN>MGN connection in the attractive
654 glomerulus VA1v (Dweck *et al.*, 2015; Knaden *et al.*, 2014; Knaden *et al.*, 2012; Mohamed *et al.*,
655 2019b; Stensmyr *et al.*, 2012). Why do aversive olfactory circuits have a stronger MGN>MGN

connection than attractive circuits? In the larval *Drosophila* AL, reciprocal LN>LN synapses induce disinhibition induced by a strong connection between the pan-glomerular LNs and a bilateral projecting LN, the Keystone LN, which synapses strongly onto pan-glomerular LNs and selectively onto OSNs, which are activated by attractive food odors. This is thought to be a key feature to switch from homogenous to heterogeneous presynaptic inhibition and therefore to a selective gain control enhancing contrast between attractive and aversive odor activation (Berck *et al.*, 2016). Such balanced inhibitory systems could also be present in the adult *Drosophila* AL, reflected in the strong LN>LN connection in DA2 and DL5. Disinhibition of interglomerular presynaptic inhibition in aversive glomeruli circuits might be important for the fly to stay vigilant to aversive odors, while perceiving attractive cues, for example during feeding conditions so that a fast switch in behavior can be initiated if necessary.

Autaptic connection within the dendritic tree of a single uPN

We observed autapses along the large dendritic tree of the single DL5-uPN. To our knowledge, this is the first report of bulk dendro-dendritic autapses in the *Drosophila* olfactory system, indicating a cell-type specific occurrence of autapses in the DL5-uPN as reported for other cell types in the optic lobe (Takemura et al., 2015). Autapses are also reported to be present at different frequencies in different types of neurons in the mammalian brain (Bacci *et al.*, 2006; Bekkers, 1998; Bekkers, 2009; Ikeda *et al.*, 2006; Saada *et al.*, 2009; Tamás *et al.*, 1997; Van der Loos *et al.*, 1972). In *Drosophila,* most uPNs are cholinergic (Croset *et al.*, 2018; Kazama *et al.*, 2008; Tanaka *et al.*, 2012; Yasuyama *et al.*, 2003; Yasuyama *et al.*, 1999) and the DL5-uPN autapses reported here might activate either nicotinic or muscarinic acetylcholine postsynaptic receptors**.** Muscarinic acetylcholine receptors have an inhibitory effect in the Kenyon cells of the mushroom body (Bielopolski *et al.*, 2019), but mediate excitation in the AL (Rozenfeld *et al.*, 2019)**.**

What could be the function of these autaptic feedback loops within the DL5-uPN dendritic tree? Recent studies in vertebrates show that excitatory autapses enhance neuron bursting and excitability (Guo *et al.*, 2016; Wiles *et al.*, 2017; Yin *et al.*, 2018). Autaptic inhibitory connections have been implicated in circuit synchronization, spike-timing precision, self-stabilization of neuronal circuits and feedback inhibition (Bacci *et al.*, 2006; Bekkers, 1998; Ikeda *et al.*; Saada *et al.*, 2009; Tamás *et al.*, 1997; Van der Loos *et al.*, 1972).

Autapses in the DL5 uPN form mainly long-distance feedback loops, connecting distinct dendritic subtrees and the basal dendrite region (closer to the soma) with distal branches. This spatial segregation is similar to the distribution of non-autaptic pre- and postsynaptic sites in *Drosophila* uPNs, where presynapses are located more frequently at basal dendrites than postsynapses (Rybak *et al.*, 2016) and other insects, such as *Periplaneta americana* and moths (Lei *et al.*, 2010; Malun, 1991; Sun *et al.*, 1997). Dendro-dendritic autaptic feedback loops connecting basal to distal branches and distinct dendritic subtrees of a large dendritic tree might facilitate

activity correlation between distant dendritic subunits, as described for non-autaptic, reciprocal uPN>uPN connections (Kazama *et al.*, 2009). This could be important in a large compartmentalized dendrite that receives inhomogeneous excitation by several OSNs at distinct dendritic sites, in order to enhance synchronized depolarization events along the dendrite, supporting signal integration (Graubard *et al.*, 1980; Tran-Van-Minh *et al.*, 2015). Clustered autapses could mediate local signal input amplification for distinct dendritic subunits (Kumar *et al.*, 2018; Liu *et al.*, 2022). Autaptic contacts, finally, could be able to shift the uPN membrane depolarization towards the spiking threshold, and enhance the firing probability during activation.

In conclusion, we provide a comprehensive comparative analysis of the ultrastructure and synaptic circuitry of two functionally diverse olfactory glomeruli with distinct computational demands, processing either single odorant information in a dedicated olfactory pathway (DA2) or input regarding several odorants and taking part in combinatory coding across distributed glomeruli (DL5). Our work provides an opportunity to gain insight into variations in network architecture and provides fundamental knowledge for future understanding of glomerular processing. By comparing our data with those from another narrowly tuned glomerulus (VA1v), we distilled prominent circuit features that suggest that narrowly tuned glomerular circuits encode odor signals with a weaker left-right-contrast, improved accuracy, stronger signal amplification and stronger intraglomerular signal modulation relative to broadly tuned glomeruli. Our findings reveal the existence of autapses in olfactory glomeruli and indicate that dendro-dendritic autapses play an important role in dendritic signal integration.

MATERIAL AND METHODS:

Fly line and fly rearing

Flies of the genotype *Orco-GAL4; UAS-GCaMP6s* were obtained from the Bloomington *Drosophila* Stock Center (https://bdsc.indiana.edu) and reared on standard *Drosophila* food at 25°C and 70% humidity on a 12 h:12 h day:night cycle. Seven-days old female flies were used. In these flies, Orco-positive olfactory sensory cells emit green fluorescence, making possible to identify individual glomeruli.

Brain dissection and fixation for Focus Ion Beam Microscopy-Scanning electron microscopy (FIB-SEM)

Two 7-day old female flies were anesthetized with nitric oxide (with Sleeper TAS; INJECT+MATIC, Switzerland) and decapitated with forceps. Heads were dipped for one minute in 0.05% Triton X-100 in 0.1M Sorensen's phosphate buffer, pH 7.3 and transferred to a droplet of freshly prepared ice-cooled fixative (2.5% glutaraldehyde and 2.0% paraformaldehyde in 0.1M Sørensen's phosphate buffer, pH 7.3; as in (Karnovsky, 1965). The proboscis was removed and the back of the head was opened to improve fixative penetration. After 5-10 minutes, the brain was dissected out of the head capsule and post-fixed for two hours on ice. Fixation was stopped by rinsing the brain several times in ice-cooled 0.1M Sørensen's phosphate buffer, pH 7.3 (after (Rybak *et al.*, 2016)).

Laser branding of glomeruli for identification during FIB-SEM microscopy

To identify the glomeruli of interest at the ultrastructural level and to limit to a minimum the volume of tissue to be scanned with FIB-SEM, near-infrared laser branding (NIRB,(Bishop *et al.*, 2011). Glomeruli of interest were first located with light microscopy in brains of *Orco-GAL4; UAS-GCaMP6s* flies using a confocal microscope (ZEISS LSM 710 NLO, Carl Zeiss, Germany), a 40x water immersion objective (W Plan-Apochromat 40x/1.0 DIC VIS-IR, Carl Zeiss, Jena, Germany), a laser wavelength of 925 nm at 30% laser power and ZEN software (Carl Zeiss, Germany). Once glomeruli DA2 or DL5 were identified by means of location, shape and size the volume of interest (VOI) was tagged with fiducial marks ("laser-branded") close to the borders of the glomerulus (**Figure 1A-B**), using an infrared Chameleon Ultra diode-pumped laser (Coherent, Santa Clara, USA) at wavelength

800 nm and at 75-90% of laser power). Two laser scan rounds were performed for each induced fiducial brand. DA2 (right AL) and DL5 (left AL) were laser-branded in the same fly. A second glomerulus DA2 was marked in the right AL of another fly.

Transmission Electron Microscopy

Brains were rinsed with 2.5% sodium-cacodylate buffer and post-fixed in 1% osmium tetroxide and 1% potassium ferrocyanide in cacodylate buffer for 2 hours. After rinsing with cacodylate buffer the brains were dehydrated with a graded acetone series (30%-100% acetone), including an additional *en bloc* staining step in-between, in which the brains were incubated in 1% uranyl acetate in 50% acetone for 30 minutes in the dark, and gradually infiltrated with Araldite (glycerol-based aromatic epoxy resins; Serva, Germany). In the final step, the tissue was embedded in pure resin and left in a 60°C incubator to polymerize for 48h. Resin blocks were trimmed with a Reichert UltraTrim microtome (Leica, USA) and the fiducial laser marks were then located in semi-thin sections. To check tissue quality before performing high-resolution volume-based electron microscopy, serial sections 50 nm in thickness were cut with a diamond knife (Ultra 45°, Diatome, Switzerland) on a Reichert Ultracut S ultramicrotome (Leica, Germany), collected on single slot grids (2 x 1 mm), and imaged with a JEM 1400 electron microscope (Jeol, Germany) operated at 80 kV. Digital micrographs were obtained with a Gatan Orius SC 1000 CCD camera (Gatan Orius SC 1000; Gatan, USA) controlled with the Gatan Microscopy Suite software Vers. 2.31.734.0.

.

Focused Ion Beam-Scanning Electron Microscopy (FIB-SEM)

Before serial Focused Ion Beam milling and Scanning Electron Microscopy imaging (FIB-SEM; (Knott *et al.*, 2008; Xu *et al.*, 2017), the surface of the trimmed block was coated with a conductive carbon layer to prevent charging artifacts. A FEI Helios NanoLab G3 UC (FEI, USA) was used for FIB-SEM process. The laser marks used to landmark the VOI were visible across the surface of the block. The VOI surface was protected via a local deposition of platinum using a gas injection system for subsequent ion and electron beam deposition. The material surrounding the VOI at the front and the side was removed to reduce re-deposition of material during FIB-SEM. Serial images across the entire VOI were generated by repeated cycles of milling slices orthogonal to the block surface via

FIB and imaging via SEM the newly exposed surface. The tissue was milled with a focused beam of gallium ions using FEI's Tomahawk ion column (accelerating voltage: 30 kV, beam current: 790 pA, milling steps: 20 nm). FEI's Elstar electron column was used to create the backscattered electron contrast images using an In-Column Detector (accelerating voltage. 3kV; 1.6 nA; dwell time: 10 µs). The DA2 and DL5 volumes in the first fly were imaged with a resolution of 4.9 x 4.9 x 20 nm^3/vox (DA2: 769 images with 4096 x 3536 pix; DL5: 976 images with 5218 x 3303 pix). The volume of a second DA2 in a second fly was imaged with a resolution of 4.4 x 4.4 x 20 nm^3/vox (571 images with 4096 x 3536 pix). The milling/imaging cycles were controlled with the Auto Slice and View 4.0 software (FEI).

Image alignment, 3D reconstruction and segmentation

FIB-SEM image stacks were aligned by maximizing the Pearson correlation coefficient of the central part of two consecutive images using template matching from the openCV library (https://opencv.org). Dense reconstructions of the glomeruli were produced by manually tracing all neuronal fibers and by annotating all synapses within the two glomeruli, using a skeleton-based reconstruction procedure similar to previous approaches (Berck *et al.*, 2016; Schneider-Mizell *et al.*, 2016; Zheng *et al.*, 2017). Up to five independent tracers and two reviewers participated in an iterative reconstruction process using the web-based reconstruction software CATMAID (http://www.catmaid.org; RRID:SCR_006278; (Saalfeld *et al.*, 2009; Schneider-Mizell *et al.*, 2016); **Figure 1D, Figure 1 -- video 1**), performing a dense reconstruction of synaptic neuropil. In a second fly, neurons of a DA2 glomerulus were manually reconstructed with the volume-based reconstruction method TrakEM2 (Cardona *et al.*, 2012), an ImageJ (Fiji) plugin (https://imagej.net/TrakEM2).

Neuron visualization

Reconstructed neurons were visualized using CATMAID 3D visualization (http://www.catmaid.org (**Figure 1 and 2**) and using Blender 3D, an open-source 3D software (https://www.blender.org/; **Figure 7 – figure supplement 1**). Neuron data from CATMAID were imported and shaded by Strahler order using an existing CATMAID plugin for Blender

(https://github.com/schlegelp/CATMAID-to-Blender; Schlegel et al., 2016). Volume-based reconstructions were visualized as surface shapes in CATMAID imported from TrakEM2 (https://imagej.net/TrakEM2).

Glomerular border definition

The definition of the boundary between olfactory glomeruli was based on the combination of several structural features: the spatial position of pre- and postsynaptic elements along OSN axons, the position of the majority of uPN postsynaptic sites, the faint glial leaflets scattered at the periphery of the glomerulus, and the fiducial laser marks (**Figure 1B, D**).

Neuron identification

Neuronal fibers were assigned to one of three pre-defined neuron classes: OSNs, uPNs, and MGNs. The classification was based on their 3D shape (**Figure 2A**), their branching intensity (**Figure 2B**), the average diameter of their fibers (neuronal profiles: **Figure 2A -** FIB-SEM image; exemplary volume-based reconstruction), the ratio of T-bars-to-input sites and the size of their T-bars, which were either “small” (few postsynaptic connections) or “large” (many postsynaptic connections **Figure 2 – supplement 1B-D)**. In addition, several intracellular features helped to classify neuron classes: the shape and appearance of mitochondria, the size and electron density of vesicles and the amount of synaptic spinules (small filopodia-like invaginations of neighboring cells (**Figure 2A -** FIB-SEM image; (Gruber *et al.*, 2018). OSNs and uPNs could be counted, due to their uniglomerular character, by means of the identification of the axons (OSNs) or main dendrites (uPNs) entering the glomerulus. The number of MGNs could not be counted because of their pan-glomerular projection patterns in the AL. Ipsi- and contralateral OSNs in DA2 and DL5 were identified based on the trajectory of axonal fibers and their entry location in each glomerulus, (example neurons: **Figure 4B).** Ipsilateral OSNs reach the glomerulus from the ipsilateral antennal nerve and leave the glomerulus towards the antennal lobe commissure (ALC: (Tanaka *et al.*, 2012). Contralateral OSNs reach the glomerulus projecting from the ALC.

Data analysis

With the aid of the web-based software CATMAID (http://www.catmaid.org) the following properties were quantified: glomerular volume, neuronal fiber length (in µm), number of fiber branching points, number of synaptic input and output sites and T-bars (see data availability). In a second fly, the volume of neurons in DA2 was measured with the aid of TrakEM2 (Cardona *et al.*, 2012), an ImageJ (Fiji) plugin (https://imagej.net/TrakEM2). The following calculations were performed:

1. $Innervation\ density = \frac{total\ neuron\ length\ (\mu m)}{glomerular\ volume\ (\mu m^3)}$,
    a. calculated as a ratio: (1) the sum of all neuronal fibers of each neuron class or (2) all together (**Table 1**) or (3) for each neuron individually (**Figure 3**)
2. $Glomerular\ synaptic\ density = \frac{\#\ of\ synaptic\ inputs,-\ outputs\ or\ T-bars}{glomerular\ volume\ (\mu m^3)}$,
    a. calculated as a ratio: (1) the sum of all neuronal fibers of each neuron class or (2) all together (**Table 1**) or (3) for each neuron individually (**Figure 3**)
3. $Neuronal\ synaptic\ density = \frac{\#\ of\ synaptic\ inputs-,outputs\ or\ T-bars}{neuronal\ fiber\ length\ (\mu m)}$ (**Table 1; Figure 3 – figure supplement 1**)
4. $Synaptic\ ratios = \frac{\#\ of\ T-bars\ or\ outputs}{inputs}$ (represents the average for each neuron class; **Table 1**)
5. $Polyadicity = \frac{\#\ of\ outputs}{T-bars}$ (represents the average number of postsynaptic sites at a T-bar of each neuron class; **Table 1 and Figure 1E**)
6. $\text{Relative differences} = \frac{respective\ value\ target\ glomerulus-value\ \ source\ \ glomerulus}{source\ glomerulus} \times 100$ (**Table S1; Table S2**)
7. $\text{Relative synaptic strength} = \frac{\#\ of\ synaptic\ contacts\ from\ neuron\ class\ A\ to\ B}{\#\ all\ synaptic\ contacts\ in\ corresponding\ glomerulus}$ (**Table S1; Table S2**)
8. $\text{Fraction of output} = \frac{\#\ of\ outputs\ of\ neuron\ class\ A\ directed\ to\ neuron\ class\ B}{total\ \#\ of outputs\ of\ neuron\ class\ A} \times 100$
9. $\text{Fraction of input} = \frac{\#\ of\ \ inputs\ from\ neuron\ class\ A\ from\ class\ B}{total\ \#\ of\ inputs\ of\ neuron\ class\ A} \times 100$

Graphs were made with the programming language R and RStudio (R Core Team, 2018) using the packages 'ggplot2' and 'reshape' (see data availability) or with Python (see data availability). All figures were compiled with Adobe Illustrator CS5 software (Adobe Inc.).

Statistical analysis was performed with R Studio (R Studio Team, 2016) using the packages 'ggsignif'. Differences between samples DA2 and DL5 or between ipsilateral and contralateral OSNs were tested for significance with a two-sided student's t-test if sample size was normally distributed, or with Wilcoxon two sample test if the data was not normally distributed (noted in figure legend). Data is in all cases represented as mean + standard deviation.

Analysis of autapses

The location of autapses, the measurement of their geodesic distance (distance along the neuronal dendrite) and the number of branching points from point A (presynaptic site) to B (postsynaptic profile) was analyzed with Python using the package 'neuroboom' https://github.com/markuspleijzier/neuroboom (see also data availability).

Data availability

Datasets will be available through the public CATMAID instance: https://catmaid.ice.mpg.de/catmaid_2020.02.15/#. Neurons are named according to their neuron classification. All data and source code packages used in this study are hosted on GitHub: https://github.com/. The neuroboom Python package was used for dendrogram analysis, available at https://github.com/markuspleijzier/neuroboom and https://pypi.org/project/neuroboom/.

Acknowledgments

The authors are most grateful to Katrin Buder for the support with electron microscopy sample preparation, and Veit Grabe for advice on two-photon imaging. Great thanks also to Albert Cardona for discussion on synaptic networks, him, and Tom Kazimiers (Kazmos GmbH) for instruction in the use of CATMAID. The neuronal reconstructions were conducted with the outstanding support of Damilola E. Akinyemi**,** Eckard E. Schumann, and Michael Adewoye. We thank Martin Nawrot and Magdalena Springer for constructive comments and discussions about autpases. The work was supported by Roland Kilper and Ute Müller (aura optics, Jena), the European Regional Development Fund, by funds from the DFG (grant no. 430592330), in the

884 Priority Program 'Evolutionary Optimisation of Neuronal Processing' (DFG-SPP 2205) and by the
885 Max Planck Society.
886
887 **Author Contributions**

888 Study concept and design: JR, BSH, RC, LG
889
890 Acquisition of data: LG, JR, MS, TP
891
892 Analysis and interpretation of data: LG, RC, JR, MP
893
894 Drafting of the manuscript: LG, RC, JR
895
896 Critical revision of the manuscript: all authors
897
898 Study supervision: RC, JR

REFERENCES

Acebes, A., & Ferrus, A. (2001). Increasing the Number of Synapses Modifies Olfactory Perception in Drosophila. *Journal of Neuroscience, 21*(16), 6264–6273.

Agarwal, G., & Isacoff, E. (2011). Specializations of a pheromonal glomerulus in the Drosophila olfactory system. *Journal of Neurophysiology, 105*(4), 1711-1721. doi:10.1152/jn.00591.2010

Ai, H., & Hagio, H. (2013). Morphological analysis of the primary center receiving spatial information transferred by the waggle dance of honeybees. *Journal of Comparative Neurology, 521*(11), 2570-2584. doi:10.1002/cne.23299

Andersson, M. N., Löfstedt, C., & Newcomb, R. D. (2015). Insect olfaction and the evolution of receptor tuning. *Frontiers in Ecology and Evolution, 3*. doi:10.3389/fevo.2015.00053

Anton, S., van Loon, J. J., Meijerink, J., Smid, H. M., Takken, W., & Rospars, J. P. (2003). Central projections of olfactory receptor neurons from single antennal and palpal sensilla in mosquitoes. *Arthropod Structure and Development, 32*(4), 319-327. doi:10.1016/j.asd.2003.09.002

Asahina, K., Louis, M., Piccinotti, S., & Vosshall, L. B. (2009). A circuit supporting concentration-invariant odor perception in Drosophila. *Journal of Biology, 8*(1), 9. doi:10.1186/jbiol108

Assisi, C., Stopfer, M., & Bazhenov, M. (2012). Excitatory Local Interneurons Enhance Tuning of Sensory Information. *PLoS Computational Biology, 8*(7), e1002563. doi:10.1371/journal.pcbi.1002563

Auer, T. O., Khallaf, M. A., Silbering, A. F., Zappia, G., Ellis, K., Álvarez-Ocaña, R., . . . Benton, R. (2020). Olfactory receptor and circuit evolution promote host specialization. *Nature*. doi:10.1038/s41586-020-2073-7

Bacci, A., & Huguenard, J. R. (2006). Enhancement of spike-timing precision by autaptic transmission in neocortical inhibitory interneurons. *Neuron, 49*(1), 119-130. doi:10.1016/j.neuron.2005.12.014

Bates, A. S., Schlegel, P., Roberts, R. J. V., Drummond, N., Tamimi, I. F. M., Turnbull, R., . . . Jefferis, G. (2020). Complete Connectomic Reconstruction of Olfactory Projection Neurons in the Fly Brain. *Current Biology, 30*(16), 3183-3199 e3186. doi:10.1016/j.cub.2020.06.042

Bekkers, J. M. (1998). Neurophysiology: are autapses prodigal synapses? *Current Biology, 8*(2), R52-55. doi:10.1016/s0960-9822(98)70033-8

Bekkers, J. M. (2009). Synaptic Transmission: Excitatory Autapses Find a Function? *Current Biology, 19*(7), R296-R298. doi:http://dx.doi.org/10.1016/j.cub.2009.02.010

Benton, R., Sachse, S., Michnick, S. W., & Vosshall, L. B. (2006). Atypical Membrane Topology and Heteromeric Function of *Drosophila* Odorant Receptors In Vivo. *PLoS Biology, 4*(2), 240-257. doi:10.1371/journal.pbio.0040020

Berck, M. E., Khandelwal, A., Claus, L., Hernandez-Nunez, L., Si, G., Tabone, C. J., . . . Cardona, A. (2016). The wiring diagram of a glomerular olfactory system. *Elife, 5*, e14859. doi:10.7554/eLife.14859

Bhandawat, V., Olsen, S. R., Gouwens, N. W., Schlief, M. L., & Wilson, R. I. (2007). Sensory processing in the *Drosophila* antennal lobe increases reliability and separability of ensemble odor representations. *Nature Neuroscience, 10*(11), 1474-1482. doi:10.1038/nn1976

942 Bielopolski, N., Amin, H., Apostolopoulou, A. A., Rozenfeld, E., Lerner, H., Huetteroth, W., . . .
943 Parnas, M. (2019). Inhibitory muscarinic acetylcholine receptors enhance aversive
944 olfactory learning in adult Drosophila. *Elife, 8*. doi:10.7554/eLife.48264
945 Bishop, D., Nikic, I., Brinkoetter, M., Knecht, S., Potz, S., Kerschensteiner, M., & Misgeld, T. (2011).
946 Near-infrared branding efficiently correlates light and electron microscopy. *Nat Meth,*
947 *8*(7), 568-570. doi:10.1038/nmeth.1622
948 Boeckh, J., Distler, P., Ernst, K. D., Hösl, M., & Malun, D. (1990). Olfactory bulb and antennal lobe.
949 In D. Schild (Ed.), *NATO ASI Series, Vol. H39: Chemosensory Information Processing* (pp.
950 201-227). Berlin, Heidelberg: Springer Verl.
951 Boeckh, J., & Tolbert, L. P. (1993). Synaptic organization and development of the antennal lobe in
952 insects. *Microscopy Research and Technique, 24*(3), 260-280.
953 doi:10.1002/jemt.1070240305
954 Borst, A., & Heisenberg, M. (1982). Osmotropotaxis inDrosophila melanogaster. *Journal of*
955 *comparative Physiology, 147*(4), 479-484. doi:10.1007/BF00612013
956 Briggman, K. L., & Denk, W. (2006). Towards neural circuit reconstruction with volume electron
957 microscopy techniques. *Current Opinion in Neurobiology, 16*(5), 562-570.
958 doi:10.1016/j.conb.2006.08.010
959 Butcher, N. J., Friedrich, A. B., Lu, Z., Tanimoto, H., & Meinertzhagen, I. A. (2012). Different
960 classes of input and output neurons reveal new features in microglomeruli of the adult
961 *Drosophila* mushroom body calyx. *Journal of Comparative Neurology, 520*(10), 2185-2201.
962 doi:10.1002/cne.23037
963 Cardona, A., Saalfeld, S., Schindelin, J., Arganda-Carreras, I., Preibisch, S., Longair, M., . . .
964 Douglas, R. J. (2012). TrakEM2 Software for Neural Circuit Reconstruction. *PLoS ONE, 7*(6),
965 e38011. doi:10.1371/journal.pone.0038011
966 Cardona, A., Saalfeld, S., Tomancak, P., & Hartenstein, V. (2009). *Drosophila* brain development:
967 closing the gap between a macroarchitectural and microarchitectural approach. *Cold*
968 *Spring Harb Symp Quant Biol, 74*, 235-248. doi:10.1101/sqb.2009.74.037
969 Chen, W. R., & Shepherd, G. M. (2005). The olfactory glomerulus: A cortical module with specific
970 functions. *Journal of Neurocytology, 34*, 353–360.
971 Chou, Y. H., Spletter, M. L., Yaksi, E., Leong, J. C., Wilson, R. I., & Luo, L. (2010). Diversity and
972 wiring variability of olfactory local interneurons in the *Drosophila* antennal lobe. *Nature*
973 *Neuroscience, 13*(4), 439-449. doi:10.1038/nn.2489
974 Christie, J. M., Bark, C., Hormuzdi, S. G., Helbig, I., Monyer, H., & Westbrook, G. L. (2005).
975 Connexin36 mediates spike synchrony in olfactory bulb glomeruli. *Neuron, 46*(5), 761-772.
976 doi:10.1016/j.neuron.2005.04.030
977 Coates, K. E., Calle-Schuler, S. A., Helmick, L. M., Knotts, V. L., Martik, B. N., Salman, F., . . . Dacks,
978 A. M. (2020). The Wiring Logic of an Identified Serotonergic Neuron That Spans Sensory
979 Networks. *The Journal of Neuroscience, 40*(33), 6309-6327. doi:10.1523/jneurosci.0552-
980 20.2020
981 Couto, A., Alenius, M., & Dickson, B. J. (2005). Molecular, anatomical, and functional organization
982 of the *Drosophila* olfactory system. *Current Biology, 15*(17), 1535-1547.
983 doi:10.1016/j.cub.2005.07.034
984 Cover, K. K., & Mathur, B. N. (2021). Axo-axonic synapses: Diversity in neural circuit function.
985 *Journal of Comparative Neurology, 529*(9), 2391-2401. doi:10.1002/cne.25087

Croset, V., Treiber, C. D., & Waddell, S. (2018). Cellular diversity in the Drosophila midbrain revealed by single-cell transcriptomics. *Elife, 7*. doi:10.7554/eLife.34550

Cuntz, H., Borst, A., & Segev, I. (2007). Optimization principles of dendritic structure. *Theor Biol Med Model, 4*, 21. doi:10.1186/1742-4682-4-21

Dacks, A. M., Christensen, T. A., & Hildebrand, J. G. (2006). Phylogeny of a serotonin-immunoreactive neuron in the primary olfactory center of the insect brain. *Journal of Comparative Neurology, 498*(6), 727-746. doi:10.1002/cne.21076

Dalal, T., Gupta, N., & Haddad, R. (2020). Bilateral and unilateral odor processing and odor perception. *Commun Biol, 3*(1), 150. doi:10.1038/s42003-020-0876-6

Datta, S. R., Vasconcelos, M. L., Ruta, V., Luo, S., Wong, A., Demir, E., . . . Axel, R. (2008). The *Drosophila* pheromone cVA activates a sexually dimorphic neural circuit. *Nature, 452*(7186), 473-477. doi:10.1038/nature06808

de Bruyne, M., Clyne, P. J., & Carlson, J. R. (1999). Odor coding in a model olfactory organ: the *Drosophila* maxillary palp. *Journal of Neuroscience, 19*(11), 4520-4532.

de Bruyne, M., Foster, K., & Carlson, J. R. (2001). Odor Coding in the *Drosophila* Antenna. *Neuron, 30*(2), 537-552. doi:10.1016/S0896-6273(01)00289-6

de la Rocha, J., Doiron, B., Shea-Brown, E., Josić, K., & Reyes, A. (2007). Correlation between neural spike trains increases with firing rate. *Nature, 448*(7155), 802-806. doi:10.1038/nature06028

Demir, M., Kadakia, N., Anderson, H. D., Clark, D. A., & Emonet, T. (2020). Walking Drosophila navigate complex plumes using stochastic decisions biased by the timing of odor encounters. *Elife, 9*. doi:10.7554/eLife.57524

Dolan, M.-J., Frechter, S., Bates, A. S., Dan, C., Huoviala, P., Roberts, R. J. V., . . . Jefferis, G. S. X. E. (2019). Neurogenetic dissection of the Drosophila lateral horn reveals major outputs, diverse behavioural functions, and interactions with the mushroom body. *Elife, 8*, e43079. doi:10.7554/eLife.43079

Dolan, M. J., Belliart-Guérin, G., Bates, A. S., Frechter, S., Lampin-Saint-Amaux, A., Aso, Y., . . . Jefferis, G. (2018). Communication from Learned to Innate Olfactory Processing Centers Is Required for Memory Retrieval in Drosophila. *Neuron, 100*(3), 651-668.e658. doi:10.1016/j.neuron.2018.08.037

Duistermars, B. J., Chow, D. M., & Frye, M. A. (2009). Flies require bilateral sensory input to track odor gradients in flight. *Current Biology, 19*(15), 1301-1307.

Dweck, H. K. M., Ebrahim, S. A. M., Thoma, M., Mohamed, A. A. M., Keesey, I. W., Trona, F., . . . Hansson, B. S. (2015). Pheromones mediating copulation and attraction in *Drosophila*. *Proceedings of the National Academy of Sciences, 112*(21), E2829-E2835. doi:10.1073/pnas.1504527112

Ebrahim, S. A. M., Dweck, H. K. M., Stökl, J., Hofferberth, J. E., Trona, F., Weniger, K., . . . Knaden, M. (2015). *Drosophila* Avoids Parasitoids by Sensing Their Semiochemicals via a Dedicated Olfactory Circuit. *PLoS Biology, 13*(12), e1002318. doi:10.1371/journal.pbio.1002318

Eckstein, N., Bates, A. S., Du, M., Hartenstein, V., Jefferis, G. S. X. E., & Funke, J. (2020). Neurotransmitter Classification from Electron Microscopy Images at Synaptic Sites in Drosophila. *bioRxiv*, 2020.2006.2012.148775. doi:10.1101/2020.06.12.148775

Eichler, K., Litwin-Kumar, A., Li, F., Park, Y., Andrade, I., Schneider-Mizell, C. M., . . . Cardona, A. (2017). The Complete Connectome Of A Learning And Memory Center In An Insect Brain. *bioRxiv*. doi:10.1101/141762

Felsenberg, J., Jacob, P. F., Walker, T., Barnstedt, O., Edmondson-Stait, A. J., Pleijzier, M. W., . . . Waddell, S. (2018). Integration of Parallel Opposing Memories Underlies Memory Extinction. *Cell, 175*(3), 709-722.e715. doi:https://doi.org/10.1016/j.cell.2018.08.021

Fiala, A. (2007). Olfaction and olfactory learning in Drosophila: recent progress. *Current Opinion in Neurobiology, 17*(6), 720-726. doi:10.1016/j.conb.2007.11.009

Fishilevich, E., & Vosshall, L. B. (2005). Genetic and functional subdivision of the *Drosophila* antennal lobe. *Current Biology, 15*(17), 1548-1553. doi:10.1016/j.cub.2005.07.066

Fröhlich, A. (1985). Freeze-Fracture Study of an Invertebrate Multiple-Contact Synapse: The Fly Photoreceptor Tetrad. *Journal of Comparative Neurology, 241*(3), 311-326. doi:10.1002/cne.902410306

Galizia, C. G. (2014). Olfactory coding in the insect brain: data and conjectures. *European Journal of Neuroscience, 39*(11), n/a-n/a. doi:10.1111/ejn.12558

Galizia, C. G., Nagler, K., Holldobler, B., & Menzel, R. (1998). Odour coding is bilaterally symmetrical in the antennal lobes of honeybees (Apis mellifera). *European Journal of Neuroscience, 10*(9), 2964-2974.

Gao, Q., Yuan, B., & Chess, A. (2000). Convergent projections of Drosophila olfactory neurons to specific glomeruli in the antennal lobe. *Nature*.

Gao, X. J., Clandinin, T. R., & Luo, L. (2015). Extremely Sparse Olfactory Inputs Are Sufficient to Mediate Innate Aversion in *Drosophila PLoS ONE, 10*(4), e0125986. doi:10.1371/journal.pone.0125986

Gaudry, Q., Hong, E. J., Kain, J., de Bivort, B. L., & Wilson, R. I. (2013). Asymmetric neurotransmitter release enables rapid odour lateralization in *Drosophila*. *Nature, 493*(7432), 424-428. doi:10.1038/nature11747

Gondré-Lewis, M. C., Park, J. J., & Loh, Y. P. (2012). Chapter Two - Cellular Mechanisms for the Biogenesis and Transport of Synaptic and Dense-Core Vesicles. In K. W. Jeon (Ed.), *International Review of Cell and Molecular Biology* (Vol. 299, pp. 27-115): Academic Press.

Goyal, R. K., & Chaudhury, A. (2013). Structure activity relationship of synaptic and junctional neurotransmission. *Autonomic Neuroscience: Basic and Clinical, 176*(1), 11-31. doi:10.1016/j.autneu.2013.02.012

Grabe, V., Baschwitz, A., Dweck, Hany K. M., Lavista-Llanos, S., Hansson, Bill S., & Sachse, S. (2016). Elucidating the Neuronal Architecture of Olfactory Glomeruli in the *Drosophila* Antennal Lobe. *Cell Reports, 16*(12), 3401-3413. doi:10.1016/j.celrep.2016.08.063

Grabe, V., & Sachse, S. (2018). Fundamental principles of the olfactory code. *BioSystems, 164*, 94-101. doi:10.1016/j.biosystems.2017.10.010

Grabe, V., Schubert, M., Strube-Bloss, M., Reinert, A., Trautheim, S., Lavista-Llanos, S., . . . Sachse, S. (2020). Odor-Induced Multi-Level Inhibitory Maps in Drosophila. *eNeuro, 7*(1). doi:10.1523/eneuro.0213-19.2019

Grabe, V., Strutz, A., Baschwitz, A., Hansson, B. S., & Sachse, S. (2015). Digital in vivo 3D atlas of the antennal lobe of *Drosophila melanogaster*. *Journal of Comparative Neurology, 523*(3), 530-544. doi:10.1002/cne.23697

Graubard, K., Raper, J. A., & Hartline, D. K. (1980). Graded synaptic transmission between spiking neurons. *Proc Natl Acad Sci U S A, 77*(6), 3733-3735. doi:10.1073/pnas.77.6.3733

Gruber, L., Rybak, J., Hansson, B. S., & Cantera, R. (2018). Synaptic Spinules in the Olfactory Circuit of Drosophila melanogaster. *Front Cell Neurosci, 12*(86), 86. doi:10.3389/fncel.2018.00086

Guo, D., Wu, S., Chen, M., Perc, M., Zhang, Y., Ma, J., . . . Yao, D. (2016). Regulation of Irregular Neuronal Firing by Autaptic Transmission. *Sci Rep, 6*, 26096. doi:10.1038/srep26096

Guven-Ozkan, T., & Davis, R. L. (2014). Functional neuroanatomy of *Drosophila* olfactory memory formation. *Learning & Memory, 21*(10), 519-526. doi:10.1101/lm.034363.114

Hallem, E. A., & Carlson, J. R. (2006). Coding of odors by a receptor repertoire. *Cell, 125*(1), 143-160. doi:10.1016/j.cell.2006.01.050

Hallem, E. A., Ho, M. G., & Carlson, J. R. (2004). The molecular basis of odor coding in the Drosophila antenna. *Cell, 117*(7), 965-979. doi:10.1016/j.cell.2004.05.012

Hansson, B. S., & Anton, S. (2000). Function and morphology of the antennal lobe: new developments. *Annual Review of Entomology, 45*, 203-231. doi:10.1146/annurev.ento.45.1.203

Hartenstein, V. (2016). The Central Nervous System of Invertebrates. In S. V. Shepherd (Ed.), *The Wiley Handbook of Evolutionary Neuroscience* (pp. 173-235).

Haverkamp, A., Hansson, B. S., & Knaden, M. (2018). Combinatorial Codes and Labeled Lines: How Insects Use Olfactory Cues to Find and Judge Food, Mates, and Oviposition Sites in Complex Environments. *Front Physiol, 9*, 49. doi:10.3389/fphys.2018.00049

Helmstaedter, M. (2013). Cellular-resolution connectomics: challenges of dense neural circuit reconstruction. *Nature Methods, 10*(6), 501-507. doi:10.1038/nmeth.2476

Hirata, Y. (1964). Some observations on the fine structure of the synapses in the olfactory bulb of the mouse, with particular reference to the atypical synaptic configurations. *Archivum histologicum japonicum, 24*(3), 293-302.

Hong, E. J., & Wilson, R. I. (2015). Simultaneous encoding of odors by channels with diverse sensitivity to inhibition. *Neuron, 85*(3), 573-589. doi:10.1016/j.neuron.2014.12.040

Horne, J. A., Langille, C., McLin, S., Wiederman, M., Lu, Z., Xu, C. S., . . . Meinertzhagen, I. A. (2018). A resource for the *Drosophila* antennal lobe provided by the connectome of glomerulus VA1v. *Elife, 7*, e37550. doi:10.7554/eLife.37550

Huang, G. B., Scheffer, L. K., & Plaza, S. M. (2018). Fully-Automatic Synapse Prediction and Validation on a Large Data Set. *Frontiers in Neural Circuits, 12*(87). doi:10.3389/fncir.2018.00087

Hulse, B. K., Haberkern, H., Franconville, R., Turner-Evans, D. B., Takemura, S.-y., Wolff, T., . . . Jayaraman, V. (2021). A connectome of the Drosophila central complex reveals network motifs suitable for flexible navigation and context-dependent action selection. *Elife, 10*, e66039. doi:10.7554/eLife.66039

Huoviala, P., Dolan, M.-J., Love, F. M., Myers, P., Frechter, S., Namiki, S., . . . Jefferis, G. S. X. E. (2020). Neural circuit basis of aversive odour processing in *Drosophila* from sensory input to descending output. 394403. doi:10.1101/394403 %J bioRxiv

Ikeda, K., & Bekkers, J. M. Autapses. *Current Biology, 16*(9), R308. doi:10.1016/j.cub.2006.03.085

Ikeda, K., & Bekkers, J. M. (2006). Autapses. *Current Biology, 16*(9), R308. doi:10.1016/j.cub.2006.03.085

Jeanne, James M., & Wilson, Rachel I. (2015). Convergence, Divergence, and Reconvergence in a Feedforward Network Improves Neural Speed and Accuracy. *Neuron, 88*(5), 1014-1026. doi:10.1016/j.neuron.2015.10.018

Jefferis, G. S., Potter, C. J., Chan, A. M., Marin, E. C., Rohlfing, T., Maurer, C. R., Jr., & Luo, L. (2007). Comprehensive maps of *Drosophila* higher olfactory centers: spatially segregated fruit and pheromone representation. *Cell, 128*(6), 1187-1203. doi:10.1016/j.cell.2007.01.040

Karnovsky, M. J. (1965). A formaldehyde-glutaraldehyde fixative of high osmolarity for use in electron microscopy. *Journal of Cellular Biology, 27*, 137.

Kazama, H., & Wilson, R. I. (2008). Homeostatic Matching and Nonlinear Amplification at Identified Central Synapses. *Neuron, 58*(3), 401-413. doi:http://dx.doi.org/10.1016/j.neuron.2008.02.030

Kazama, H., & Wilson, R. I. (2009). Origins of correlated activity in an olfactory circuit. *Nature Neuroscience, 12*(9), 1136-1144. doi:10.1038/nn.2376

Keene, A. C., & Waddell, S. (2007). Drosophila olfactory memory: single genes to complex neural circuits. *Nature Reviews: Neuroscience, 8*(5), 341-354.

Keesey, I. W., & Hansson, B. S. (2021). 10 - The neuroethology of labeled lines in insect olfactory systems. In G. J. Blomquist & R. G. Vogt (Eds.), *Insect Pheromone Biochemistry and Molecular Biology (Second Edition)* (pp. 285-327). London: Academic Press.

Keesey, I. W., Zhang, J., Depetris-Chauvin, A., Obiero, G. F., Knaden, M., & Hansson, B. S. (2019). Evolution of a pest: towards the complete neuroethology of Drosophila suzukii and the subgenus Sophophora. *bioRxiv*, 717322. doi:10.1101/717322

Knaden, M., & Hansson, B. S. (2014). Mapping odor valence in the brain of flies and mice. *Current Opinion in Neurobiology, 24*(1), 34-38. doi:10.1016/j.conb.2013.08.010

Knaden, M., Strutz, A., Ahsan, J., Sachse, S., & Hansson, B. S. (2012). Spatial representation of odorant valence in an insect brain. *Cell Reports, 1*, 392-399. doi:10.1016/j.celrep.2012.03.002

Knott, G., Marchman, H., & Lich, B. (2008). Serial Section Scanning Electron Microscopy of Adult Brain Tissue Using Focused Ion Beam Milling. *Journal of Neuroscience, 28*(12), 2964-2959. doi:10.1523/JNEUROSCI.3189-07.2008

Kreher, S. A., Mathew, D., Kim, J., & Carlson, J. R. (2008). Translation of sensory input into behavioral output via an olfactory system. *Neuron, 59*(1), 110-124. doi:10.1016/j.neuron.2008.06.010

Kumar, A., Schiff, O., Barkai, E., Mel, B. W., Poleg-Polsky, A., & Schiller, J. (2018). NMDA spikes mediate amplification of inputs in the rat piriform cortex. *Elife, 7*, e38446. doi:10.7554/eLife.38446

Kurtovic, A., Widmer, A., & Dickson, B. J. (2007). A single class of olfactory neurons mediates behavioural responses to a Drosophila sex pheromone. *Nature, 446*(7135), 542-546. doi:10.1038/nature05672

Laissue, P. P., Reiter, C., Hiesinger, P. R., Halter, S., Fischbach, K. F., & Stocker, R. F. (1999). Three-dimensional reconstruction of the antennal lobe in *Drosophila melanogaster*. *The Journal of Comparative Neurology, 405*(4), 543-552. doi:10.1002/(sici)1096-9861(19990322)405:4<543::aid-cne7>3.0.co;2-a

Laissue, P. P., & Vosshall, L. B. (2008). The Olfactory Sensory Map in *Drosophila*. In G. M. Technau (Ed.), *Brain Development in Drosophila melanogaster* (pp. 102-114). New York: Springer.

Lei, H., Oland, L. A., Riffell, J. A., Beyerlein, A., & Hildebrand, J. G. (2010). Microcircuits for Olfactory Information Processing in the Antennal Lobe of *Manduca sexta*. In G. M. Shepherd & S. Grillner (Eds.), *Handbook of Brain Microcircuits* (pp. 417-426). New York: Oxford University Press.

Li, F., Lindsey, J. W., Marin, E. C., Otto, N., Dreher, M., Dempsey, G., . . . Rubin, G. M. (2020). The connectome of the adult Drosophila mushroom body provides insights into function. *Elife, 9*. doi:10.7554/eLife.62576

Li, H., Horns, F., Wu, B., Xie, Q., Li, J., Li, T., . . . Luo, L. (2017). Classifying Drosophila Olfactory Projection Neuron Subtypes by Single-Cell RNA Sequencing. *Cell, 171*(5), 1206-1220.e1222. doi:https://doi.org/10.1016/j.cell.2017.10.019

Li, P. H., Lindsey, L. F., Januszewski, M., Zheng, Z., Bates, A. S., Taisz, I., . . . Jain, V. (2020). Automated Reconstruction of a Serial-Section EM *Drosophila* Brain with Flood-Filling Networks and Local Realignment. *bioRxiv*, 605634. doi:10.1101/605634

Liang, L., & Luo, L. (2010). The olfactory circuit of the fruit fly *Drosophila melanogaster*. *Sci China Life Sci, 53*(4), 472-484. doi:10.1007/s11427-010-0099-z

Lin, S., Kao, C.-F., Yu, H.-H., Huang, Y., & Lee, T. (2012). Lineage analysis of Drosophila lateral antennal lobe neurons reveals notch-dependent binary temporal fate decisions. *PLoS Biology, 10*(11), e1001425-e1001425. doi:10.1371/journal.pbio.1001425

Liu, T. X., Davoudian, P. A., Lizbinski, K. M., & Jeanne, J. M. (2022). Connectomic features underlying diverse synaptic connection strengths and subcellular computation. *Current Biology, 32*(3), 559-569.e555. doi:https://doi.org/10.1016/j.cub.2021.11.056

Liu, W. W., & Wilson, R. I. (2013). Glutamate is an inhibitory neurotransmitter in the *Drosophila* olfactory system. *Proceedings of the National Academy of Sciences, 110*(25), 10294–10299. doi:10.1073/pnas.1220560110

Malun, D. (1991). Inventory and distribution of synapses of identified uniglomerular projection neurons in the antennal lobe of Periplaneta americana. *Journal of Comparative Neurology, 305*(2), 348-360. doi:10.1002/cne.903050215

Malun, D., Waldow, U., Kraus, D., & Boeckh, J. (1993). Connections between the Deutocerebrum and the Protocerebrum, and Neuroanatomy of Several Classes of Deutocerebral Projection Neurons in the Brain of Male Periplaneta-Americana. *Journal of Comparative Neurology, 329*(2), 143-162.

Marin, E. C., Büld, L., Theiss, M., Sarkissian, T., Roberts, R. J. V., Turnbull, R., . . . Jefferis, G. (2020). Connectomics Analysis Reveals First-, Second-, and Third-Order Thermosensory and Hygrosensory Neurons in the Adult Drosophila Brain. *Current Biology, 30*(16), 3167-3182.e3164. doi:10.1016/j.cub.2020.06.028

Masse, N. Y., Turner, G. C., & Jefferis, G. S. (2009). Olfactory information processing in Drosophila. *Current Biology, 19*(16), R700-713. doi:10.1016/j.cub.2009.06.026

Masson, C., & Mustaparta, H. (1990). Chemical information processing in the olfactory system of insects. *Physiological Review, 70(1)*, 199-245.

McTavish, T., Migliore, M., Shepherd, G., & Hines, M. (2012). Mitral cell spike synchrony modulated by dendrodendritic synapse location. *Frontiers in Computational Neuroscience, 6*. doi:10.3389/fncom.2012.00003

Meinertzhagen, I. A. (2018). Of what use is connectomics? A personal perspective on the *Drosophila* connectome. *Journal of Experimental Biology, 221*(10), jeb164954. doi:10.1242/jeb.164954 %J The Journal of Experimental Biology

Meinertzhagen, I. A., & O'Neil, S. D. (1991). Synaptic organization of columnar elements in the lamina of the wild type in Drosophila melanogaster. *Journal of Comparative Neurology, 305*, 232-263.

Miroschnikow, A., Schlegel, P., Schoofs, A., Hueckesfeld, S., Li, F., Schneider-Mizell, C. M., . . . Pankratz, M. J. (2018). Convergence of monosynaptic and polysynaptic sensory paths onto common motor outputs in a Drosophila feeding connectome. *Elife, 7*, e40247. doi:10.7554/eLife.40247

Mohamed, A. A. M., Hansson, B. S., & Sachse, S. (2019a). Third-Order Neurons in the Lateral Horn Enhance Bilateral Contrast of Odor Inputs Through Contralateral Inhibition in Drosophila. *Front Physiol, 10*, 851. doi:10.3389/fphys.2019.00851

Mohamed, A. A. M., Retzke, T., Das Chakraborty, S., Fabian, B., Hansson, B. S., Knaden, M., & Sachse, S. (2019b). Odor mixtures of opposing valence unveil inter-glomerular crosstalk in the Drosophila antennal lobe. *Nat Commun, 10*(1), 1201. doi:10.1038/s41467-019-09069-1

Mosca, T. J., & Luo, L. (2014). Synaptic organization of the *Drosophila* antennal lobe and its regulation by the Teneurins. *Elife, 3*(3), e03726. doi:10.7554/eLife.03726

Münch, D., & Galizia, C. G. (2016). DoOR 2.0 - Comprehensive Mapping of Drosophila melanogaster Odorant Responses. *Scientific Reports, 6*, 21841. doi:10.1038/srep21841 http://www.nature.com/articles/srep21841#supplementary-information

Nässel, D. R., Enell, L. E., Santos, J. G., Wegener, C., & Johard, H. A. (2008). A large population of diverse neurons in the Drosophila central nervous system expresses short neuropeptide F, suggesting multiple distributed peptide functions. *BMC Neuroscience, 9*, 90. doi:10.1186/1471-2202-9-90

Nässel, D. R., & Homberg, U. (2006). Neuropeptides in interneurons of the insect brain. *Cell and Tissue Research, 326*(1), 1-24. doi:10.1007/s00441-006-0210-8

Ng, M., Roorda, R. D., Lima, S. Q., Zemelman, B. V., Morcillo, P., & Miesenböck, G. (2002). Transmission of Olfactory Information between Three Populations of Neurons in the Antennal Lobe of the Fly. *Neuron, 36*(3), 463-474. doi:10.1016/s0896-6273(02)00975-3

Norgate, M., Lee, E., Southon, A., Farlow, A., Batterham, P., Camakaris, J., & Burke, R. (2006). Essential Roles in Development and Pigmentation for the *Drosophila* Copper Transporter DmATP7. *Molecular Biology of the Cell, 17*(1), 475-484. doi:10.1091/mbc.E05-06-0492

Okada, R., Awasaki, T., & Ito, K. (2009). Gamma-aminobutyric acid (GABA)-mediated neural connections in the *Drosophila* antennal lobe. *Journal of Comparative Neurology, 514*(1), 74-91. doi:10.1002/cne.21971

Olsen, S. R., & Wilson, R. I. (2008). Lateral presynaptic inhibition mediates gain control in an olfactory circuit. *Nature, 452*(7190), 956-960. doi:10.1038/nature06864

Otto, N., Pleijzier, M. W., Morgan, I. C., Edmondson-Stait, A. J., Heinz, K. J., Stark, I., . . . Waddell, S. (2020). Input Connectivity Reveals Additional Heterogeneity of Dopaminergic Reinforcement in Drosophila. *Current Biology, 30*(16), 3200-3211.e3208. doi:https://doi.org/10.1016/j.cub.2020.05.077

Owald, D., & Waddell, S. (2015). Olfactory learning skews mushroom body output pathways to steer behavioral choice in Drosophila. *Current Opinion in Neurobiology, 35*, 178-184. doi:10.1016/j.conb.2015.10.002

Parthasarathy, K., & Bhalla, U. S. (2013). Laterality and symmetry in rat olfactory behavior and in physiology of olfactory input. *Journal of Neuroscience, 33*(13), 5750-5760. doi:10.1523/jneurosci.1781-12.2013

Prokop, A., & Meinertzhagen, I. A. (2006). Development and structure of synaptic contacts in Drosophila. *Seminars in Cell & Developmental Biology, 17*(1), 20-30. doi:10.1016/j.semcdb.2005.11.010

Ronchi, P., Mizzon, G., Machado, P., D'Imprima, E., Best, B. T., Cassella, L., . . . Schwab, Y. (2021). High-precision targeting workflow for volume electron microscopy. *Journal of Cell Biology, 220*(9). doi:10.1083/jcb.202104069

Root, C. M., Masuyama, K., Green, D. S., Enell, L. E., Nassel, D. R., Lee, C. H., & Wang, J. W. (2008). A presynaptic gain control mechanism fine-tunes olfactory behavior. *Neuron, 59*(2), 311-321. doi:10.1016/j.neuron.2008.07.003

Rospars, J.-P., Grémiaux, A., Jarriault, D., Chaffiol, A., Monsempes, C., Deisig, N., . . . Martinez, D. (2014). Heterogeneity and Convergence of Olfactory First-Order Neurons Account for the High Speed and Sensitivity of Second-Order Neurons. *PLoS Computational Biology, 10*(12), e1003975. doi:10.1371/journal.pcbi.1003975

Rozenfeld, E., Lerner, H., & Parnas, M. (2019). Muscarinic Modulation of Antennal Lobe GABAergic Local Neurons Shapes Odor Coding and Behavior. *Cell Rep, 29*(10), 3253-3265.e3254. doi:10.1016/j.celrep.2019.10.125

Rybak, J. (2013). Exploring Brain Connectivity in Insect Model Systems of Learning and Memory. In R. Menzel & P. Benjamin (Eds.), *Invertebrate Learning and Memory* (pp. 26-40). San Diego: Academic Press.

Rybak, J. (2016). Perspective-Brain atlases for studying neuronal circuitry in arthropods. In A. Schmidt-Rhaesa, S. Harzsch, & G. Purschke (Eds.), *Structure and Evolution of Invertebrate Nervous Systems* (Vol. 1). New York: Oxford University Press.

Rybak, J., & Hansson, B. S. (2018). Olfactory Microcircuits in *Drosophila Melanogaster*. In G. M. Shepherd & S. Grillner (Eds.), *Handbook of Brain Microcircuits* (2nd ed., pp. 361-367). Oxford, UK: Oxford University Press.

Rybak, J., Talarico, G., Ruiz, S., Arnold, C., Cantera, R., & Hansson, B. S. (2016). Synaptic circuitry of identified neurons in the antennal lobe of *Drosophila melanogaster*. *Journal of Comparative Neurology, 524*(9), 1920-1956. doi:10.1002/cne.23966

Saada, R., Miller, N., Hurwitz, I., & Susswein, A. J. (2009). Autaptic excitation elicits persistent activity and a plateau potential in a neuron of known behavioral function. *Current Biology, 19*(6), 479-484. doi:10.1016/j.cub.2009.01.060

Saalfeld, S., Cardona, A., Hartenstein, V., & Tomančák, P. (2009). CATMAID: collaborative annotation toolkit for massive amounts of image data. *Bioinformatics, 25*(15), 1984-1986. doi:10.1093/bioinformatics/btp266

Sachse, S., & Galizia, C. G. (2002). Role of inhibition for temporal and spatial odor representation in olfactory output neurons: a calcium imaging study. *Journal of Neurophysiology, 87*(2), 1106-1117.

Sachse, S., & Hansson, B. S. (2016). Research spotlight: Olfactory coding in *Drosophila melanogaster*. In A. Schmidt-Rhaesa, S. Harzsch, & G. Purschke (Eds.), *Structure and Evolution of Invertebrate Nervous Systems* (pp. 640-645). Oxford: Oxford University Press.

Sachse, S., & Manzini, I. (2021). Editorial for the special issue "Olfactory Coding and Circuitries". *Cell and Tissue Research, 383*(1), 1-6. doi:10.1007/s00441-020-03389-1

Scheffer, L. K., Xu, C. S., Januszewski, M., Lu, Z., Takemura, S.-y., Hayworth, K. J., . . . Plaza, S. M. (2020). A connectome and analysis of the adult Drosophila central brain. *Elife, 9*, e57443. doi:10.7554/eLife.57443

Schlegel, P., Bates, A. S., Stürner, T., Jagannathan, S. R., Drummond, N., Hsu, J., . . . Jefferis, G. S. X. E. (2021). Information flow, cell types and stereotypy in a full olfactory connectome. *Elife, 10*, e66018. doi:10.7554/eLife.66018

Schneider-Mizell, C. M., Gerhard, S., Longair, M., Kazimiers, T., Li, F., Zwart, M. F., . . . Cardona, A. (2016). Quantitative neuroanatomy for connectomics in *Drosophila*. *Elife, 5*, e12059. doi:10.7554/eLife.12059

Seki, Y., Dweck, H. K. M., Rybak, J., Wicher, D., Sachse, S., & Hansson, B. S. (2017). Olfactory coding from the periphery to higher brain centers in the Drosophila brain. *BMC Biology, 15*(1), 56. doi:10.1186/s12915-017-0389-z

Seki, Y., Rybak, J., Wicher, D., Sachse, S., & Hansson, B. S. (2010). Physiological and morphological characterization of local interneurons in the *Drosophila* antennal lobe. *Journal of Neurophysiology, 104*(2), 1007-1019. doi:jn.00249.2010 [pii]
10.1152/jn.00249.2010

Semmelhack, J. L., & Wang, J. W. (2009). Select Drosophila glomeruli mediate innate olfactory attraction and aversion. *Nature, 459*(7244), 218-223.

Shanbhag, S. R., Muller, B., & Steinbrecht, R. A. (1999). Atlas of olfactory organs of *Drosophila melanogaster* - 1. Types, external organization, innervation and distribution of olfactory sensilla. *International Journal of Insect Morphology & Embryology, 28*(4), 377-397. doi:Doi 10.1016/S0020-7322(99)00039-2

Shepherd, G. M. (2011). The Olfactory Bulb: A Simple System in the Mammalian Brain *Comprehensive Physiology*: John Wiley & Sons, Inc.

Shepherd, G. M., Rowe, T. B., & Greer, C. A. (2021). An Evolutionary Microcircuit Approach to the Neural Basis of High Dimensional Sensory Processing in Olfaction. *Frontiers in Cellular Neuroscience, 15*. doi:10.3389/fncel.2021.658480

Silbering, A. F., & Galizia, C. G. (2007). Processing of odor mixtures in the Drosophila antennal lobe reveals both global inhibition and glomerulus-specific interactions. *Journal of Neuroscience, 27*(44), 11966-11977. doi:10.1523/jneurosci.3099-07.2007

Silbering, A. F., Okada, R., Ito, K., & Galizia, C. G. (2008). Olfactory information processing in the *Drosophila* antennal lobe: anything goes? *Journal of Neuroscience, 28*(49), 13075-13087. doi:10.1523/JNEUROSCI.2973-08.2008

Silbering, A. F., Rytz, R., Grosjean, Y., Abuin, L., Ramdya, P., Jefferis, G. S., & Benton, R. (2011). Complementary Function and Integrated Wiring of the Evolutionarily Distinct *Drosophila* Olfactory Subsystems. *Journal of Neuroscience, 31*(38), 13357-13375. doi:10.1523/JNEUROSCI.2360-11.2011

Stensmyr, M. C., Dweck, H. K., Farhan, A., Ibba, I., Strutz, A., Mukunda, L., . . . Hansson, B. S. (2012). A conserved dedicated olfactory circuit for detecting harmful microbes in *Drosophila*. *Cell, 151*(6), 1345-1357. doi:10.1016/j.cell.2012.09.046

Stocker, R. F., Lienhard, M. C., Borst, A., & Fischbach, K. F. (1990). Neuronal architecture of the antennal lobe in Drosophila melanogaster. *Cell and Tissue Research, 262*(1), 9-34.

Stocker, R. F., Singh, R. N., Schorderet, M., & Siddiqi, O. (1983). Projection patterns of different types of antennal sensilla in the antennal glomeruli of Drosophila melanogaster. *Cell and Tissue Research, 232*(2), 237-248. doi:10.1007/bf00213783

Strutz, A., Soelter, J., Baschwitz, A., Farhan, A., Grabe, V., Rybak, J., . . . Sachse, S. (2014). Decoding odor quality and intensity in the *Drosophila* brain. *Elife, 3*, e04147. doi:10.7554/eLife.04147

Su, C.-Y., Menuz, K., & Carlson, J. R. (2009). Olfactory Perception: Receptors, Cells, and Circuits. *Cell, 139*(1), 45-59. doi:10.1016/j.cell.2009.09.015

Suh, G. S. B., Wong, A. M., Hergarden, A. C., Wang, J. W., Simon, A. F., Benzer, S., . . . Anderson, D. J. (2004). A single population of olfactory sensory neurons mediates an innate avoidance behaviour in *Drosophila*. *Nature, 431*(7010), 854-859. doi:http://www.nature.com/nature/journal/v431/n7010/suppinfo/nature02980_S1.html

Sun, X. J., Tolbert, L. P., & Hildebrand, J. G. (1997). Synaptic organization of the uniglomerular projection neurons of the antennal lobe of the moth *Manduca sexta*: a laser scanning confocal and electron microscopic study. *Journal of Comparative Neurology, 379*(1), 2-20.

Szyszka, P., & Galizia, C. G. (2015). Olfaction in Insects. In R. L. Doty (Ed.), *Handbook of Olfaction and Gustation* (3 ed., pp. 531-546): John Wiley & Sons, Inc.

Taisz, I., Donà, E., Münch, D., Bailey, S. N., Morris, W. J., Meechan, K. I., . . . Galili, D. S. (2022). Generating parallel representations of position and identity in the olfactory system. *bioRxiv*, 2022.2005.2013.491877. doi:10.1101/2022.05.13.491877

Takemura, S.-y., Xu, C. S., Lu, Z., Rivlin, P. K., Parag, T., Olbris, D. J., . . . Scheffer, L. K. (2015). Synaptic circuits and their variations within different columns in the visual system of Drosophila. *Proceedings of the National Academy of Sciences, 112*(44), 13711-13716. doi:10.1073/pnas.1509820112

Tamás, G., Buhl, E. H., & Somogyi, P. (1997). Massive Autaptic Self-Innervation of GABAergic Neurons in Cat Visual Cortex. *The Journal of Neuroscience, 17*(16), 6352-6364. doi:10.1523/jneurosci.17-16-06352.1997

Tanaka, N. K., Endo, K., & Ito, K. (2012). The organization of antennal lobe-associated neurons in the adult *Drosophila* melanogaster brain. *Journal of Comparative Neurology, 520*(18), 4067-4130. doi:10.1002/cne.23142

Thoma, M., Hansson, B. S., & Knaden, M. (2015). High-resolution Quantification of Odor-guided Behavior in Drosophila melanogaster Using the Flywalk Paradigm. *J Vis Exp*(106), e53394. doi:10.3791/53394

Tobin, W. F., Wilson, R. I., & Lee, W.-C. A. (2017). Wiring variations that enable and constrain neural computation in a sensory microcircuit. *Elife, 6*, e24838. doi:10.7554/eLife.24838

Tran-Van-Minh, A., Cazé, R. D., Abrahamsson, T., Cathala, L., Gutkin, B. S., & DiGregorio, D. A. (2015). Contribution of sublinear and supralinear dendritic integration to neuronal computations. *Frontiers in Cellular Neuroscience, 9*. doi:10.3389/fncel.2015.00067

Trujillo-Cenoz, O. (1969). Some Aspects of the Structural Organization of the Medulla in Muscoid Flies l. *J Ultrastructural Research, 27*, 533-553.

Van der Loos, H., & Glaser, E. M. (1972). Autapses in neocortex cerebri: synapses between a pyramidal cell's axon and its own dendrites. *Brain Research, 48*, 355-360. doi:10.1016/0006-8993(72)90189-8

Vosshall, L. B., Wong, A. M., & Axel, R. (2000). An olfactory sensory map in the fly brain. *Cell, 102*(2), 147-159. doi:10.1016/S0092-8674(00)00021-0

Wang, J. W. (2012). Presynaptic modulation of early olfactory processing in *Drosophila*. *Developmental Neurobiology, 72*(1), 87-99. doi:10.1002/dneu.20936

Wicher, D., & Miazzi, F. (2021). Functional properties of insect olfactory receptors: ionotropic receptors and odorant receptors. *Cell and Tissue Research, 383*(1), 7-19. doi:10.1007/s00441-020-03363-x

Wiles, L., Gu, S., Pasqualetti, F., Parvesse, B., Gabrieli, D., Bassett, D. S., & Meaney, D. F. (2017). Autaptic Connections Shift Network Excitability and Bursting. *Sci Rep, 7*, 44006. doi:10.1038/srep44006

Wilson, R. I. (2013). Early Olfactory Processing in Drosophila: Mechanisms and Principles. *Annual Review of Neuroscience, 36*, 217-241. doi:10.1146/annurev-neuro-062111-150533

Xu, C. S., Hayworth, K. J., Lu, Z., Grob, P., Hassan, A. M., García-Cerdán, J. G., . . . Hess, H. F. (2017). Enhanced FIB-SEM systems for large-volume 3D imaging. *Elife, 6*, e25916. doi:10.7554/eLife.25916

Xu, C. S., Januszewski, M., Lu, Z., Takemura, S.-y., Hayworth, K. J., Huang, G., . . . Plaza, S. M. (2020). A Connectome of the Adult *Drosophila* Central Brain. 2020.2001.2021.911859. doi:10.1101/2020.01.21.911859 %J bioRxiv

Yang, K., Liu, T., Wang, Z., Liu, J., Shen, Y., Pan, X., . . . Zhang, K. (2022). Classifying Drosophila olfactory projection neuron boutons by quantitative analysis of electron microscopic reconstruction. *iScience, 25*(5), 104180. doi:https://doi.org/10.1016/j.isci.2022.104180

Yasuyama, K., Meinertzhagen, I. A., & Schurmann, F. W. (2003). Synaptic connections of cholinergic antennal lobe relay neurons innervating the lateral horn neuropile in the brain of *Drosophila melanogaster*. *Journal of Comparative Neurology, 466*(3), 299-315. doi:10.1002/cne.10867

Yasuyama, K., & Salvaterra, P. M. (1999). Localization of choline acetyltransferase-expressing neurons in *Drosophila* nervous system. *Microscopy Research and Technique, 45*(2), 65-79.

Yin, L., Zheng, R., Ke, W., He, Q., Zhang, Y., Li, J., . . . Shu, Y. (2018). Autapses enhance bursting and coincidence detection in neocortical pyramidal cells. *Nature Communications, 9*(1), 4890. doi:10.1038/s41467-018-07317-4

Yokoi, M., Mori, K., & Nakanishi, S. (1995). Refinement of odor molecule tuning by dendrodendritic synaptic inhibition in the olfactory bulb. *Proceedings of the National Academy of Sciences, 92*(8), 3371-3375. doi:doi:10.1073/pnas.92.8.3371

Zheng, Z., Lauritzen, J. S., Perlman, E., Robinson, C. G., Nichols, M., Milkie, D., . . . Bock, D. D. (2017). A Complete Electron Microscopy Volume Of The Brain Of Adult Drosophila melanogaster. *bioRxiv*. doi:10.1101/140905

Zheng, Z., Lauritzen, J. S., Perlman, E., Robinson, C. G., Nichols, M., Milkie, D., . . . Bock, D. D. (2018). A Complete Electron Microscopy Volume of the Brain of Adult Drosophila melanogaster. *Cell, 174*(3), 730-743.e722. doi:https://doi.org/10.1016/j.cell.2018.06.019

FIGURES

Figure 1: A correlative approach to analyze the ultrastructure of identified olfactory glomeruli
A-B: Two-photon laser scans of the antennal lobes in *Orco-Gal4; UAS-GCaMP6s* flies where Orco-positive olfactory sensory neurons (OSNs) in the glomerular neuropils were labeled by GCaMP (green fluorescence). Glomeruli DA2 (A) and DL5 (B) are encircled. Schematics show their relative position in the antennal lobe. Once the glomeruli of interest were identified, glomerular borders were marked with fiducial marks (white triangles) via laser branding, which enabled their identification at the ultrastructural level. **C-D**: Representative images of the same glomeruli (DA2 in **C** and DL5 in **D**) obtained with focused-ion-beam electron microscopy (FIB-SEM), showing their ultrastructure. Asterisks indicate the main neurite of uniglomerular projection neurons entering the glomerulus. White triangle shows a 2-photon laser mark (see also **A** and **B**). **E**: FIB-SEM image of a polyadic synapse: the presynaptic site (red arrowhead) is composed of a T-bar shaped presynaptic density surrounded by small vesicles and is opposed by several postsynaptic profiles (cyan dots). Scheme of a tetrad synapse: a presynaptic site with its T-bar (red arrowhead) forms four output connections (arrows) with four postsynaptic input sites (cyan dots). **F:** A skeleton-based reconstruction of an OSN axon terminal (green line) with presynaptic (red dots) and postsynaptic sites (cyan dots). The dark grey shading surrounding the OSN trace represents the volume-based reconstruction of the same neuron. Tracing and reconstruction were performed within the FIB-SEM dataset (light grey area).

Figure 2: Neuron classification and neuronal composition of the DA2 and DL5 glomeruli
A: Example FIB-SEM images (left column), volumetric neuronal reconstructions (middle column), and skeleton-based neuron traces (right column) of a representative example of each neuron class: OSNs (green), uniglomerular projection neurons (uPNs, red) and multiglomerular neurons (MGNs, blue). The ultrastructure of neurons, including T-bars (black triangle), mitochondria (asterisks) and spinules (white triangle) are indicated. Exemplar volumetric reconstructions (middle column) show the general morphology of each neuron class. Presynapses and postsynapses are indicated with red and cyan dots on the skeleton traces (right column). **B:** Average branching intensity (branching points per µm of neuronal-fiber length) of each neuron class OSNs, uPNs and MGNs in DA2 and DL5. Data represent mean+ standard deviation (error bars). Data points represent single values. Means were compared using Wilcoxon two-sample test. No significant differences of branching points/µm in OSNs or MGNs between glomeruli were found (significance was not tested for uPNs due to the presence of a single uPN in DL5). **C**: Schematic summary indicating, for each glomerulus, its volume (in μm^3), the number of neurons of each class (MGNs were not counted), the total fiber length of all neurons for each neuron class and the total number of single synaptic contacts for each glomerulus.

Table 1. Glomerular innervation and synaptic composition
Quantitative neuronal data comparing glomeruli DA2 and DL5, detailing glomerular innervation and synaptic properties for each neuronal class: OSNs (green), uPNs (red) and MGNs (blue) and the sum of all of them. **Row 1**: Total length of all neurons of each neuron class and total length for all neurons in each glomerulus. **Row 2-4**: Synaptic counts: input sites (inputs), output sites (outputs)

and T-bars (T-bars). **Row 5**: Innervation density: total neuron length (µm; row 1)/glomerular volume (µm^3); glomerular volume: DA2=1500 µm^3 and DL5=2700 µm^3 (see Figure 1C). **Row 6-8**: Total synaptic density per unit of glomerular volume (µm^3): sum of all input sites (inputs), output sites (outputs) and T-bars of each neuron class or of all neurons/glomerular volume. **Row 9-11**: Average synaptic density along neuronal fibers (illustrated also in Figure 3 – supplement 1): number of inputs, outputs or T-bars/neuron length (µm). **Row 12-13:** Average synaptic ratios: the ratio of T-bars-to-inputs or outputs-to-inputs. **Row 14:** Polyadicity: the average number of postsynaptic sites at each T-bar in DA2 and DL5. The ratios in rows 12-14 were calculated based on synaptic counts normalized to neuron length (rows 9-11). The color shading highlights values that have a relative difference greater than 20% (see relative differences Table S1) between DA2 and DL5. Dark shades highlights values that are greater in DA2 than in DL5 (green (OSNs), red (uPNs), blue (MGNs)) and light colors highlight values that are less in DA2 than in DL5.

Figure 3: Innervation density and synaptic density in DA2 and DL5

A-E: The average glomerular innervation density of OSNs (**A**), uPNs (**B**), MGNs (**C**) and collectively of all glomerular neurons (**D**); the average synaptic density of input sites (inputs), output sites (outputs) and T-bars and the average polyadicity. Innervation density: length (µm) of each neuronal fiber normalized to one µm^3 of glomerular (glom.) volume. Synaptic density: number of input sites, output sites or T-bars of each neuronal fiber normalized to one µm^3 of glomerular volume. Polyadicity: average number of single output sites per T-bar in each neuronal fiber. Data for DA2 shown in dark colors and for DL5 in light colors. Number of neurons in DA2: OSNs (green) n= 44; uPNs (red) n= 7; MGNs (blue) n=180; all neurons n=231, in DL5: OSNs n=46; uPN n=1; MGNs n=221; all neurons n=268. Data represent mean + standard deviation (error bars). Data points represent single values. Means were compared using either Student's t-test (OSNs) or Wilcoxon two-sample test (MGNs and all neurons). uPNs were not compared, since the DL5 has only one. Significance value: $p>0.05$ (not significant, no star), $p\leq0.05$ (*), $p\leq0.01$ (**), $p\leq0.001$ (***). Values are provided at data availability; polyadicity values are listed in Table 1, row 14.

Figure 4: Lateralization of OSN terminals in the antennal lobes

A: Illustration of an ipsilateral (dark green) and a contralateral (light green) OSN with dendrites in the corresponding antennae and their axonal projections to the ipsilateral olfactory glomerulus in the antennal lobe (AL) (dashed rectangle). **B**: Exemplary skeleton traces of an ipsilateral (dark green) and a contralateral (light green) OSN terminal inside glomerulus DA2. The ipsilateral OSN axons reach the glomerulus via the ipsilateral antennal nerve (arrow down) and leave the glomerulus towards the AL commissure (arrow up) while OSN axons originating at the contralateral antenna reach the glomerulus via the AL commissure. Red dots: presynapses; blue dots: postsynapses. **C**: Boxplots showing the fraction of synaptic output to uPNs (in red), - to OSNs (in green) or - toMGNs (in blue), , for the ipsilateral OSNs (dark green boxplot) and contralateral OSNs (light green), respectively, in the DA2, DL5 and VA1v glomeruli (VA1v data obtained from Horne et al., 2018). **D**: Boxplots showing the fraction of synaptic input of the same ipsilateral and contralateral OSNs that they receive from OSNs and MGNs. Connection polarity is indicated by arrows in the schematic neuronal drawings on the left of each plot. Dots represent single values.

Means were compared using either Student's T-test. Significance value: p>0.05 (not significant, no star)), p≤0.05 (*), p≤0.01 (**), p≤0.001 (***). Mean and Median values are provided at data availability.

Figure 5: Strength of synaptic connections between neuron classes in the circuitry of DA2, DL5 and VA1v.

A: Schematic representation of principal connection motifs between the neuron classes OSNs (green), uPNs (red) and MGNs (blue). The synaptic flow directed towards uPNs is a feedforward and that directed towards OSNs or from uPNs to MGNs defined as a feedback connection (arrows). **B-D**: Alluvial diagrams of the glomerular circuitry in DA2 (**B**), DL5 (**C**) and VA1v (**D**). Each diagram shows the relative synaptic strength calculated as the proportion of 1:1 single synaptic contacts between each neuron class in relation to the total number of synaptic contacts in their respective glomerulus. The synaptic strength between each neuron class, given as percentage, is indicated by the thickness of the lines. The proportions (as percentage) of output (left side) or input (right side) are illustrated by colored rectangles to the left or right of each alluvial diagram. The total number of synaptic contacts is indicated below the diagrams. Percentages of the relative synaptic strength and synaptic counts are listed in the supplementary Table S1. **E:** Stacked bar charts depict output (E') and input (E'') fractions (given as percentages) of each neuron class: OSNs (green), uPNs (red), MGNs (blue), schematically illustrated next to the bar charts respectively, to each of the other neuron classes for glomeruli DA2, DL5 and VA1v. Fractions are color-coded according to the neuron class of the respective connecting partner.

Figure 6: Differences in connectivity strength in glomeruli DA2, DL5 and VA1v

A: Schematic representation of synaptic connection motifs (arrows) between OSNs (green), uPNs (red), and MGNs (blue) in glomeruli DA2, DL5 and VA1v. The number of neurons of each class or truncated neuronal fibers (in brackets) is noted in the corresponding circle. **B**: Schematics of connection motifs (left) that are jointly stronger or weaker in DA2 and VA1v than in DL5. The relative differences (as percentage) between DA2 and DL5 as well as VA1v and DL5 are illustrated as arrows up (stronger) or arrows down (weaker) according to their intensity (see legend at the bottom) from the perspective of the target glomerulus (defined in the table header). The values of relative differences are listed in the Table S2.

Figure 7: Distribution of pre- and postsynaptic partners of autapses in the uPN dendrite of the DL5

A: Distribution of autaptic presynaptic (red dots) and postsynaptic sites (cyan dots) mapped in a dendrogram of the dendrite of the single uPN in glomerulus DL5. The basal root node (black dot) represents the entry site of the uPN dendrite into the glomerulus (closest point to its soma). Clustering of autaptic input sites along some branches are encircled. **B**: Simplified representation of the uPN's dendrogram illustrating the distinct strahler orders, at distal branches (1-4) and at basal branches (5-8); see legend on the right). **C**: Distribution of autaptic presynaptic (left) and postsynaptic input sites (right) along the dendrite, as proportions at each corresponding strahler order (color coded). Note that autaptic postsynaptic sites are located almost exclusively at the most distal dendritic branches. **D**: Dendrogram of the DL5-uPN showing the distribution of presynaptic sites (triangles) and postsynaptic sites (circles) of selected autapses (indicated by same

color). Distant pairs of pre- and postsynapses (long geodesic distance) are indicated by numbers whereas closely attached synaptic sites (short geodesic distance) are encircled and labelled with letters. **E**: Schematic of the dendrogram illustrating the location of the presynaptic (red dot) and postsynaptic (cyan dot) sites of a single autapse, the geodesic distance between them, i.e. the distance along the dendrite (µm), and the number of branching points (orange dots) between the pre- and postsynaptic components of the same autapse. **F**: Number of autapses with distinct geodesic distances between their pre- and postsynapses (illustrated in E). **G**: Number of autapses with the number of branch points between their pre- and postsynapses counted along the uPN dendrite (illustrated in E).

Horne, J.A., Langille, C., Mclin, S., Wiederman, M., Lu, Z., Xu, C.S., Plaza, S.M., Scheffer, L.K., Hess, H.F., and Meinertzhagen, I.A. (2018). A resource for the *Drosophila* antennal lobe provided by the connectome of glomerulus VA1v. *Elife* 7**,** e37550.

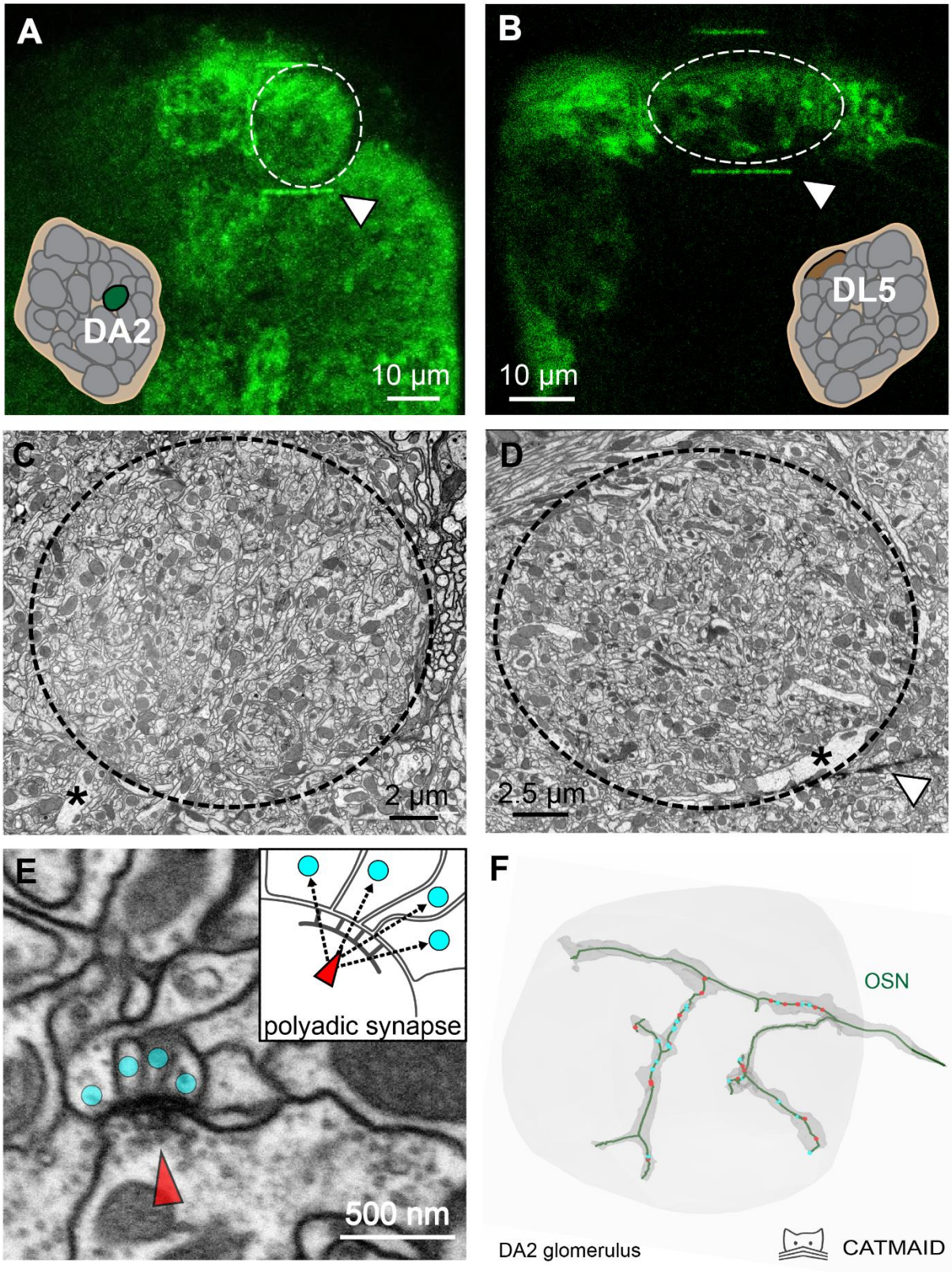

Figure 1

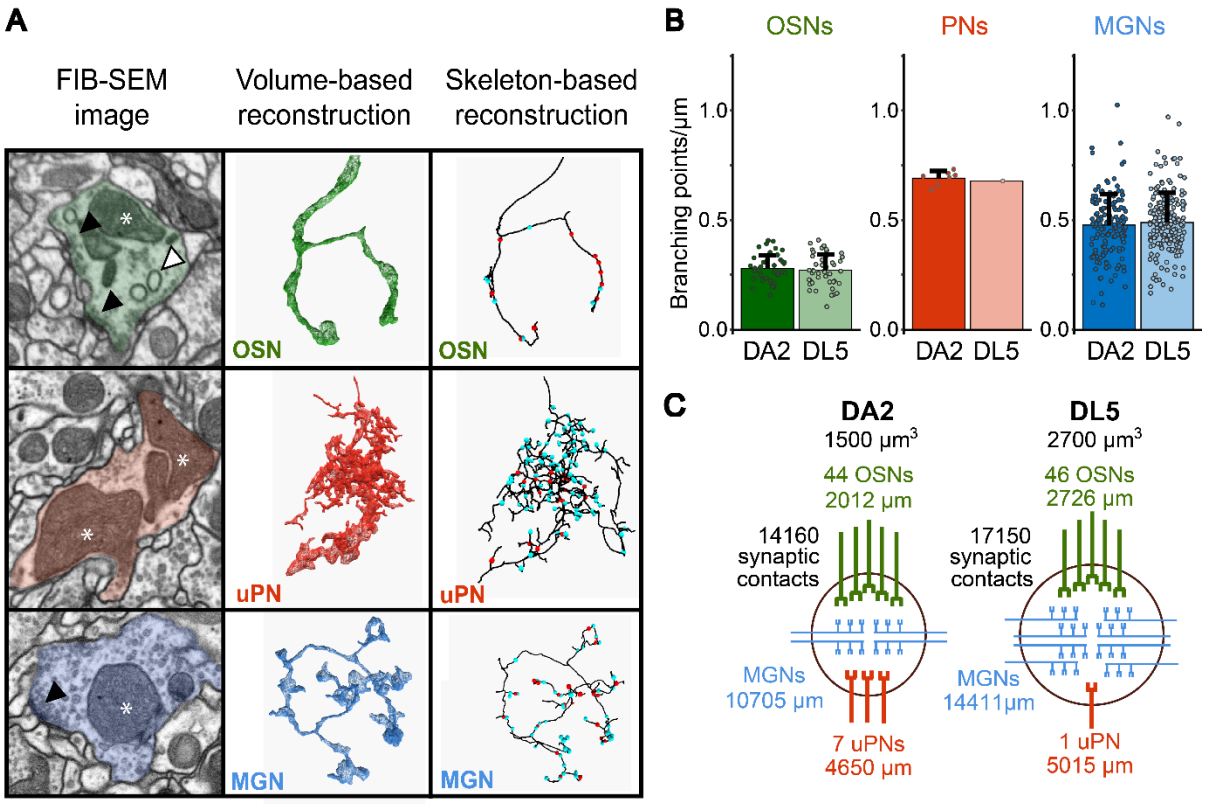

Figure 2

Row	Values	Unit	OSNs		uPNs		MGNs		all neurons	
			DA2	DL5	DA2	DL5	DA2	DL5	DA2	DL5
1	Total neuronal length	µm	2012	2727	4652	5015	10705	14411	17370	22153
2	Total synaptic counts	input	868	1083	3887	3955	7229	9018	11984	14056
3		output	6671	6828	1624	3108	5659	6749	13954	16685
4		T-bars	1063	1213	322	602	1263	1572	2648	3387
5	Total innervation density (sum of length of all neuronal fibers/glomerular volume)	µm/µm^3	1.26	1.05	2.91	1.93	6.69	5.54	10.86	8.52
6	Total glomerular synaptic density (total synaptic counts/glomerular volume)	inputs/µm^3	0.54	0.42	2.43	1.52	4.52	3.47	7.49	5.41
7		outputs/µm^3	4.17	2.63	1.02	1.20	3.54	2.60	8.72	6.42
8		T-bars/µm^3	0.66	0.47	0.20	0.23	0.79	0.60	1.66	1.30
9	Neuronal synaptic density (synaptic counts/neuronal length)	inputs/µm	0.42	0.39	0.83	0.79	0.62	0.59	0.59	0.56
10		outputs/µm	3.37	2.62	0.33	0.62	0.52	0.51	1.06	0.87
11		T-bars/µm	0.53	0.46	0.07	0.12	0.12	0.12	0.19	0.18
12	Synaptic ratio	T-bars/inputs	1.31	1.27	0.08	0.15	0.23	0.24	0.43	0.42
13		outputs/inputs	8.29	7.29	0.40	0.79	1.04	1.11	2.40	2.37
14	Polyadicity	outputs/T-bars	6.35	5.70	4.95	5.16	3.22	2.64	3.88	3.17

Table 1

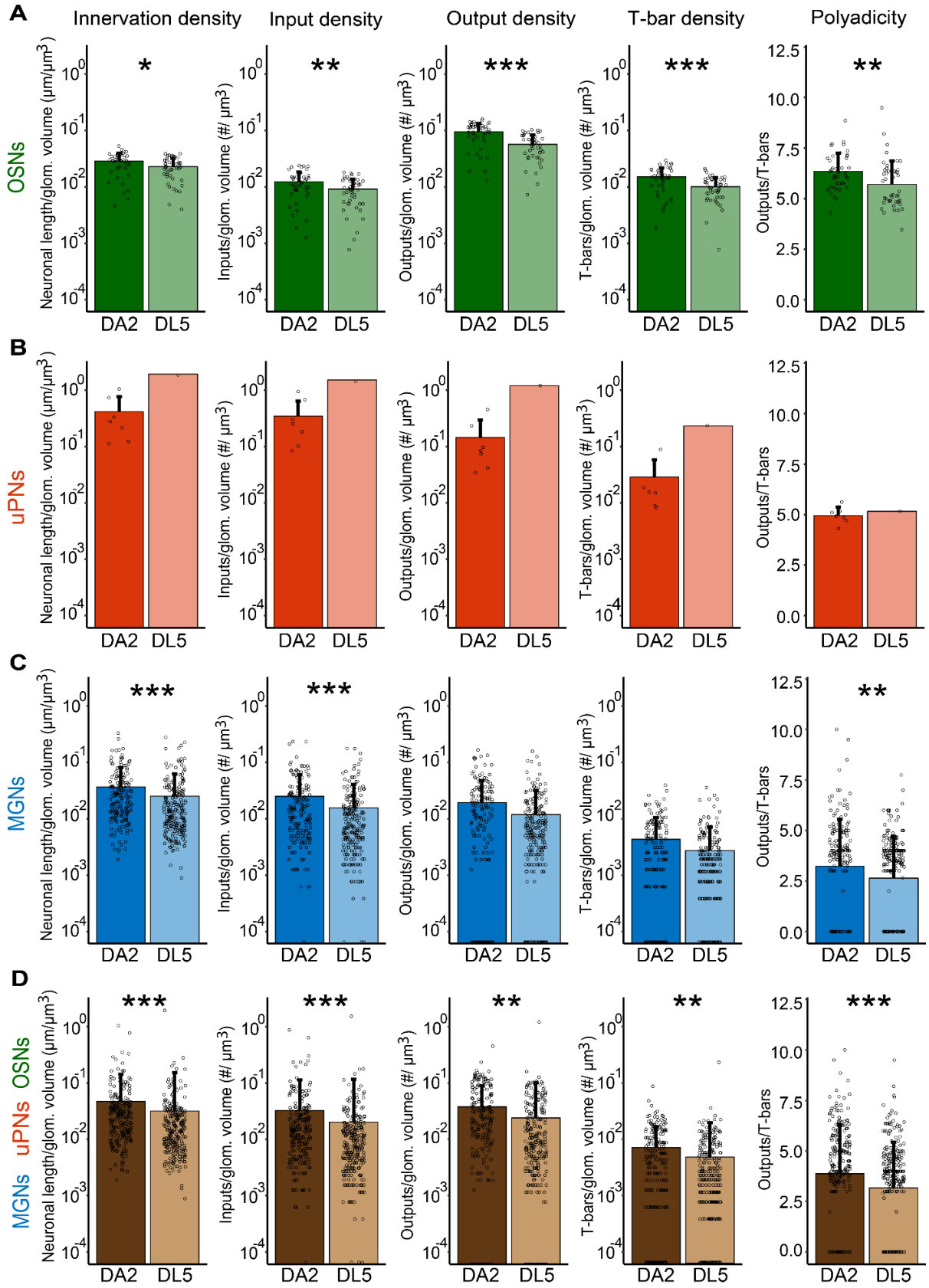

Figure 3

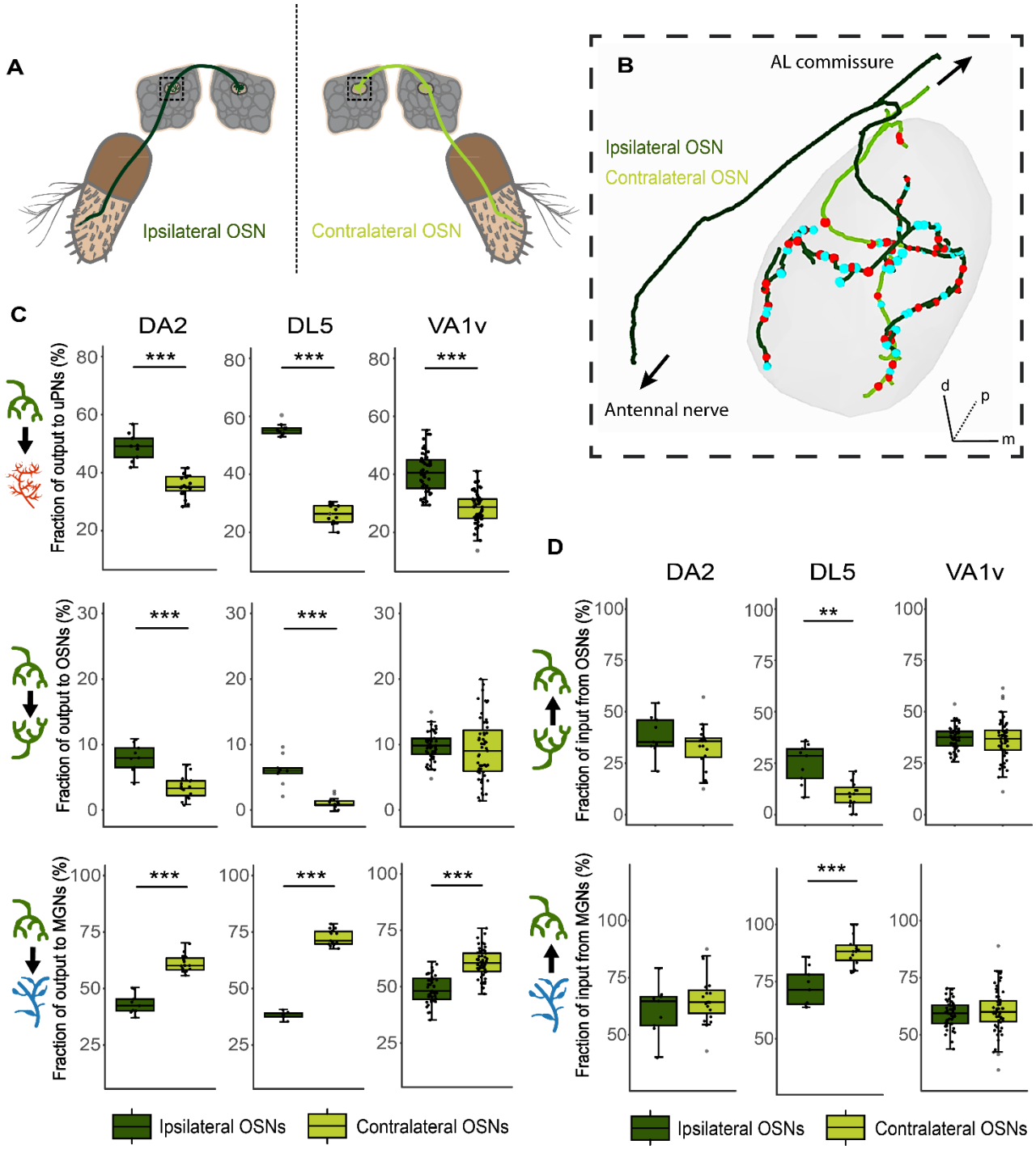

Figure 4

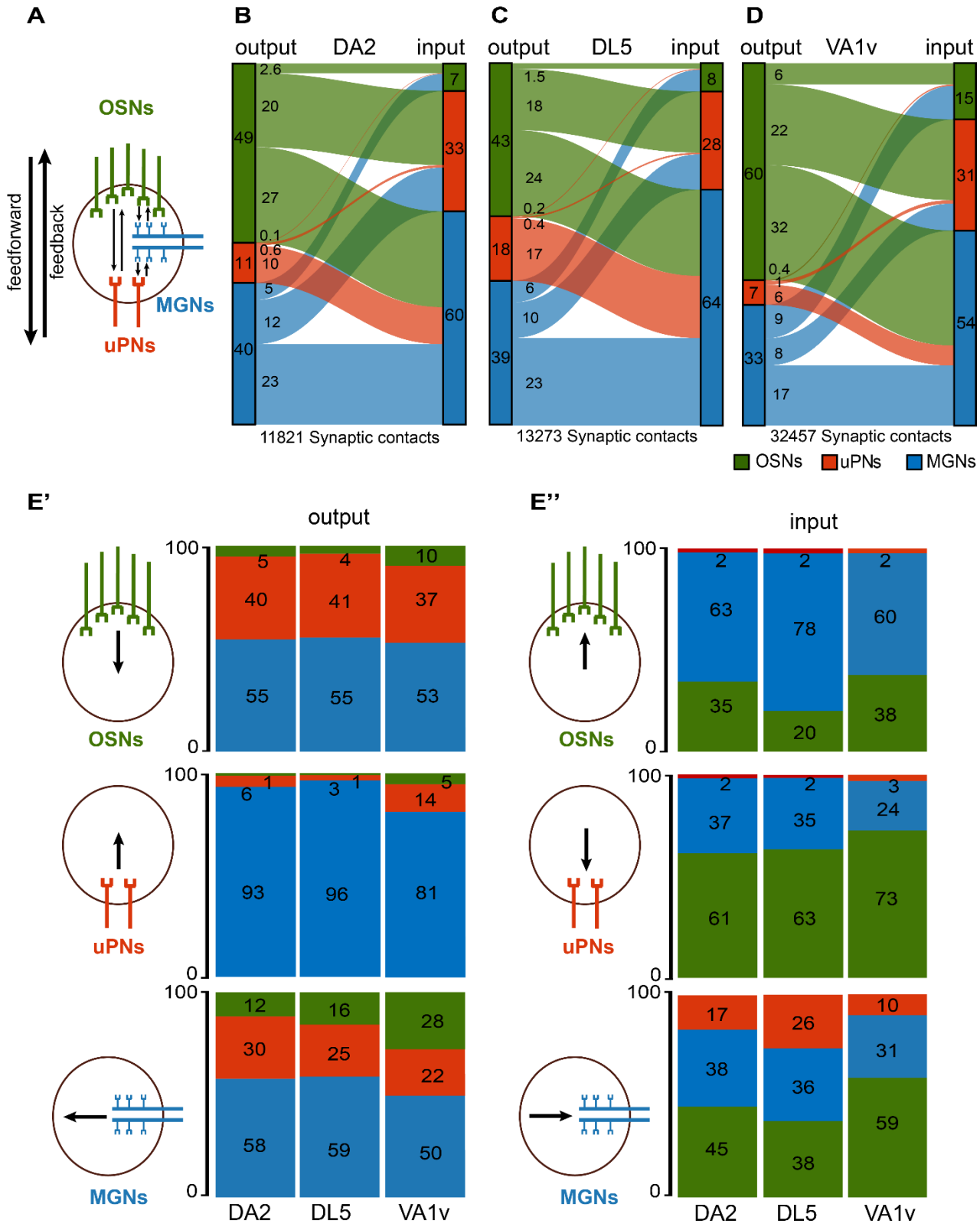

Figure 5

1590

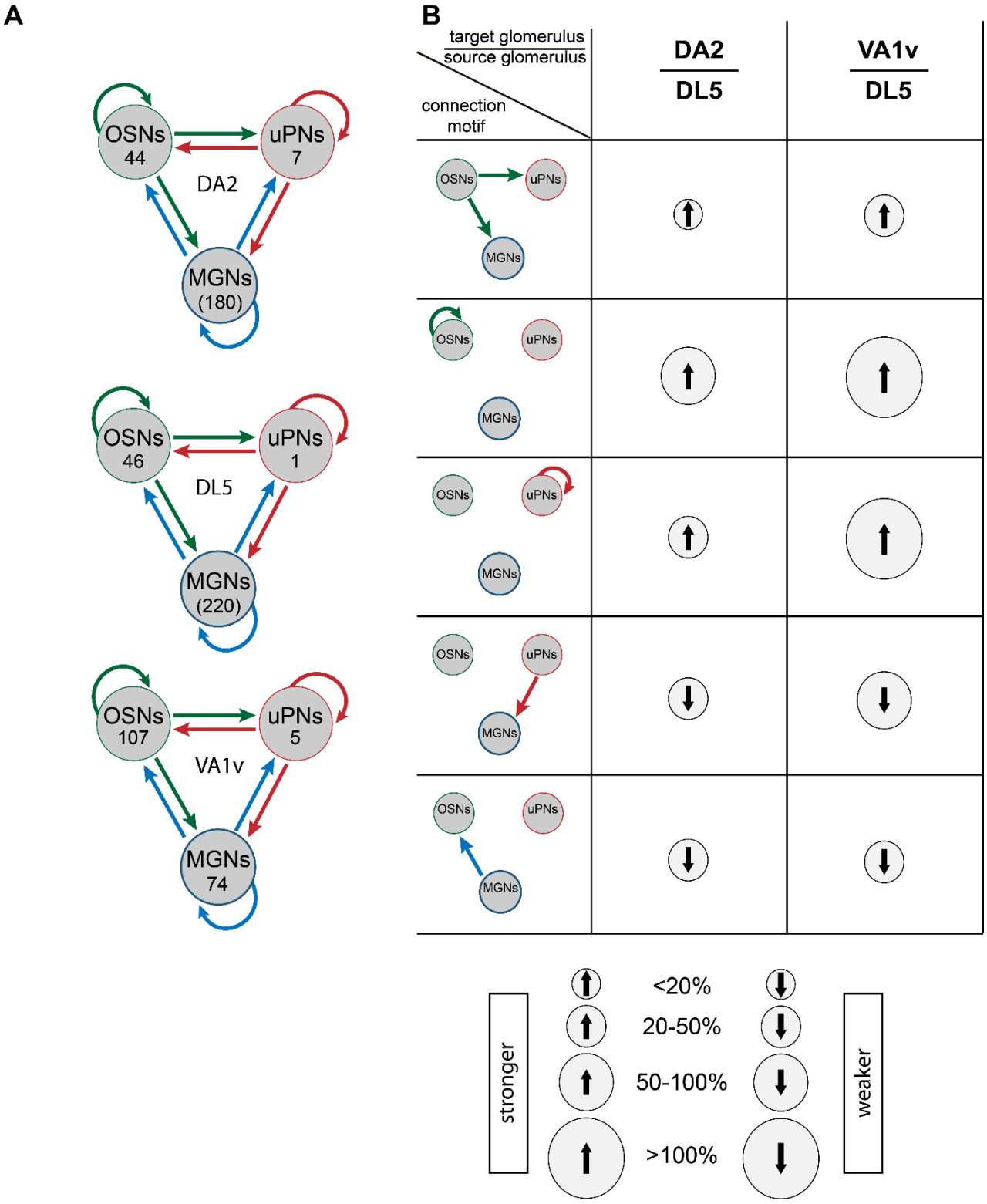

1591

1592 **Figure 6**

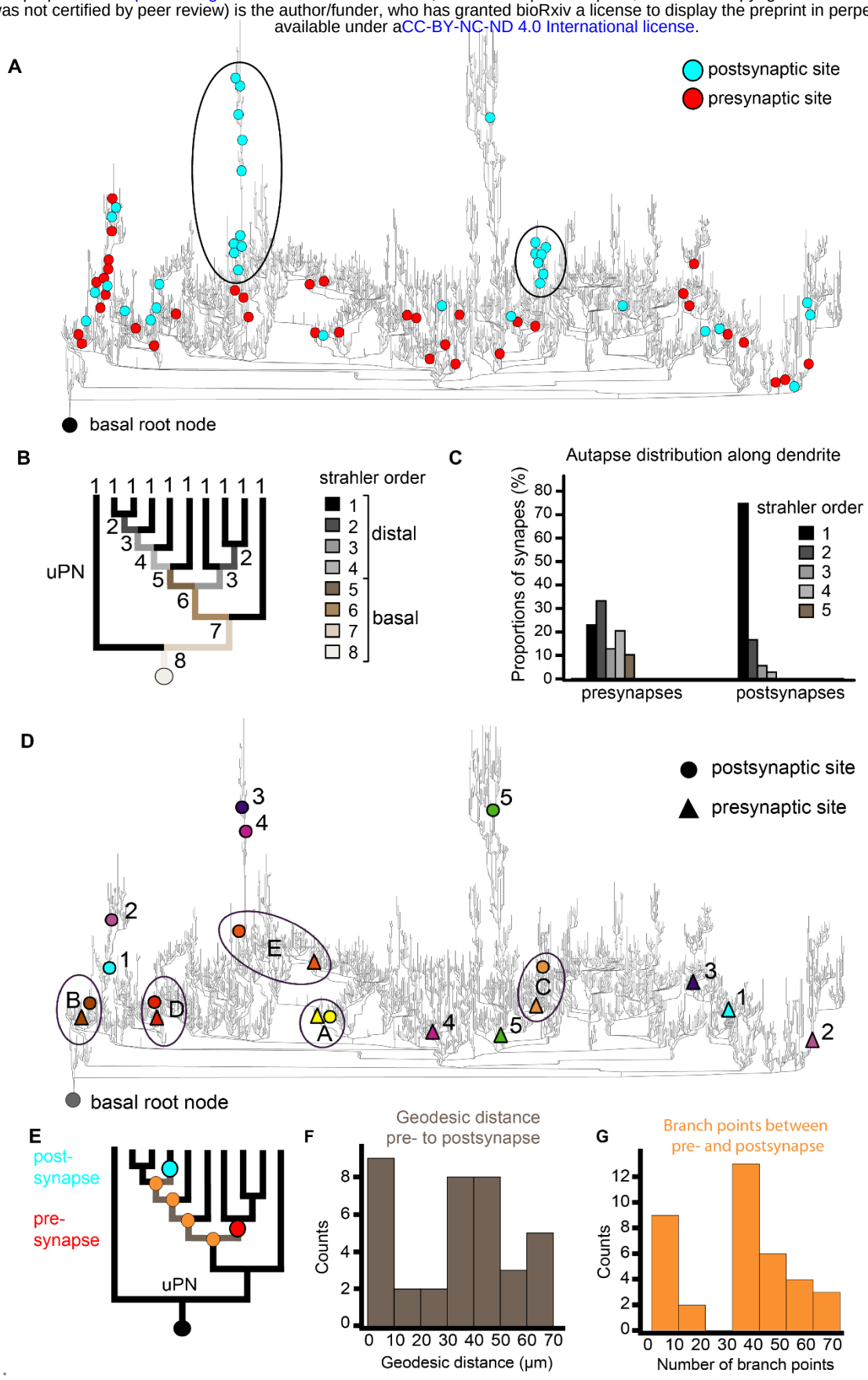

Figure 7